

Highly bright and stable NIR-BRET with blue-shifted coelenterazine derivatives for deep-tissue imaging of molecular events *in vivo*

Ryo Nishihara^{1,2#}, Ramasamy Paulmurugan^{2#}, Takahiro Nakajima³, Eiji Yamamoto⁴, Arutselvan Natarajan², Rayhaneh Afjei², Yuki Hiruta¹, Naoko Iwasawa¹, Shigeru Nishiyama¹, Daniel Citterio¹, Moritoshi Sato³, Sung Bae Kim^{2,5,*} and Koji Suzuki^{1,*}

1. Department of Applied Chemistry, Faculty of Science and Technology, Graduate School of Science and Technology, Keio University, 3-14-1 Hiyoshi, Kohoku-ku, Yokohama, Kanagawa 223-8522, Japan.
2. Molecular Imaging Program at Stanford, Bio-X Program, Stanford University School of Medicine, Palo Alto, California 94304, United States
3. Graduate School of Arts and Sciences, The University of Tokyo, 3-8-1, Komaba Meguro-ku, Tokyo 153-8902, Japan.
4. Graduate School of Science and Technology, Keio University, 3-14-1 Hiyoshi, Kohoku-ku, Yokohama, Kanagawa 223-8522, Japan.
5. Research Institute for Environmental Management Technology, National Institute of Advanced Industrial Science and Technology (AIST), 16-1 Onogawa, Tsukuba 305-8569, Japan

Equal contribution

* **Corresponding authors:**

suzuki@applc.keio.ac.jp

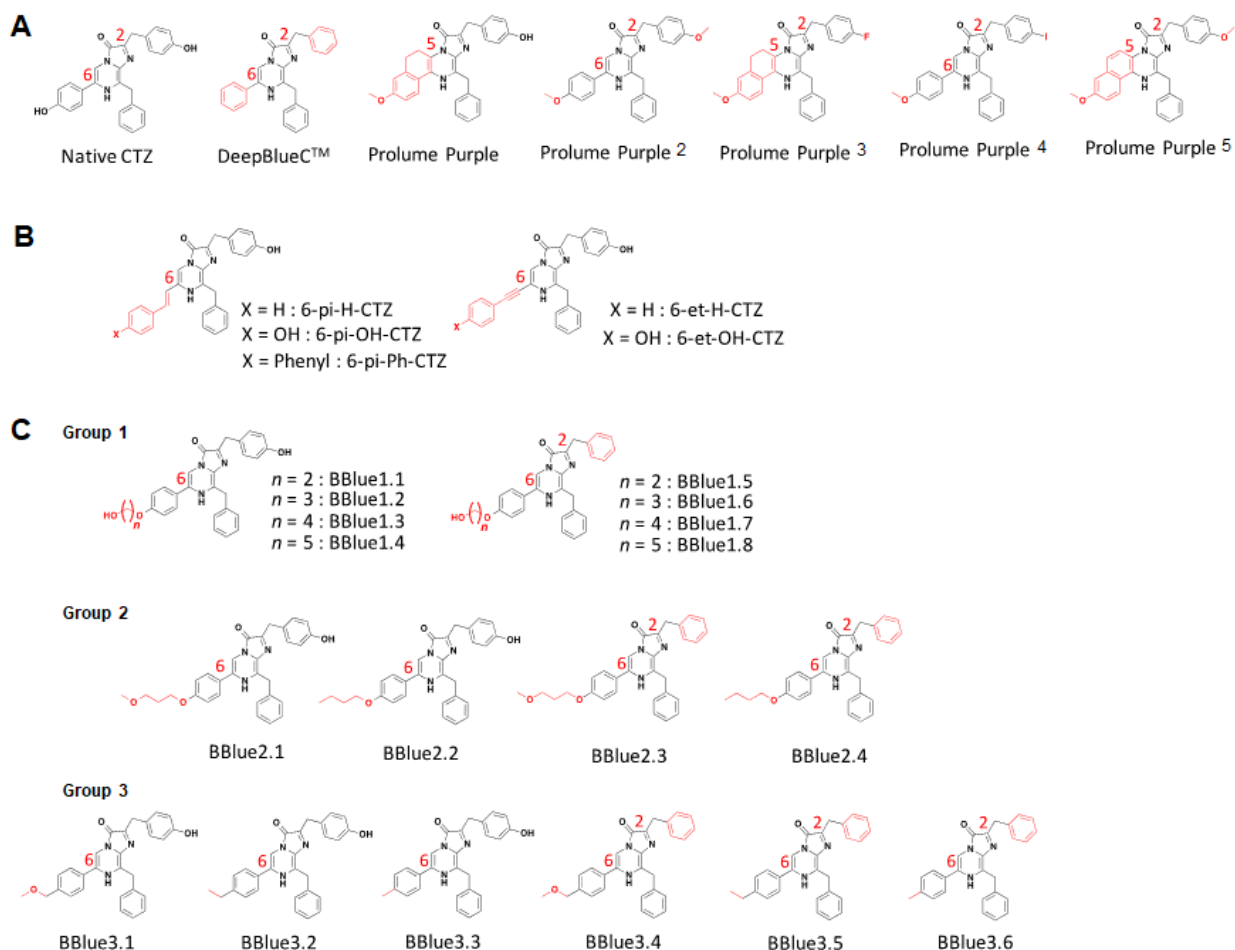
kimu-sb@aist.go.jp

Contents

1. Coelenterazine derivatives
2. Synthesis
3. Chemiluminescence assay
4. Bioluminescence assay
5. Docking simulation study
6. Bioluminescence assay with caged luciferin
7. Construction of mammalian expression plasmids for BRET imaging
8. Discussion on BRET efficiency
9. References

1. Coelenterazine derivatives

1.1. Chemical Structure of coelenterazine derivatives



Suppl. Figure 1. The detailed chemical structures of various CTZ derivatives that were synthesized and used in this study. **(A)** Native-CTZ (nCTZ) and its commercially available blue-shifted analogues: DeepBlueC (DBlueC), Prolume Purple, Prolume Purple 2, Prolume Purple 3, Prolume Purple 4, Prolume Purple 5; **(B)** 6-pi-CTZ series [1][2], 6-et-CTZ series [2]; **(C)** The novel new CTZ derivatives, named “Bottle Blue (BBlue)” synthesized for this study are categorized into 3 groups such as, BBlue1, BBlue2, and BBlue3 series: Group 1

(BBlue 1.1 - 1.8) contains a terminal hydroxyl group at C-6 position of nCTZ); Group 2 (BBlue 2.1 to BBlue 2.4) shares the terminally alkylated structures, and Groups 3 (BBlue 3.1 - 3.6) lacks the oxygen atom at the C-6 position. The characteristic functional groups in the chemical structures are highlighted in red.

1.2. Molecular design of CTZ derivatives

Coelenterazine (CTZ) is a common substrate for marine luciferases such as, *Gaussia* luciferase (GLuc), *Renilla* luciferase (RLuc) and Artificial Luciferase (ALuc), and a principle ingredient for bioluminescence (BL) light emission. More than three decades, many CTZ derivatives have been synthesized, but still remain a challenging subject in identifying optimal substrate with competent BL properties to Firefly luciferase with D-Luciferin for *in vivo* imaging. Although the crystal structure of RLuc8 (a mutant variant of RLuc) including coelenteramide (CTMD: an oxidized form of CTZ) has been reported [3] [4], the CTMD in the crystal structure is located at a “secondary binding” position and not at the position of the CTMD/CTZ during the enzymatic reaction (Figure 1A). We previously reported that the modification of the C-6 position of nCTZ by comparably bulky substituents (Suppl. Figure 1B; 6-pi-X-CTZ, where “pi” indicates a styryl group and “X” indicates any functional group at the C-6 position of CTZ) displayed significant BL emission with RLuc8 and RLuc8.6-535 [1] [2], although most of synthetic CTZs in history reduces their BLIs. The precedent studies lead us to focus on developing new derivatives of CTZ by introducing modification on the C-6 position rather than the other positions such as the C-2, C-5, and C-8.

In contrast to the 6-pi-X-CTZ series, we previously reported that the 6-et-X-CTZ series substrates emit marginally low BLI with RLuc variants (Suppl. Figure 1B; “et” means an ethynyl group at C-6 position), although they produced efficient luminescence with ALucs [2]. This luciferase selectivity

may be interpreted as the rigidity at the C-6 position causes steric hindrance with the key amino acid residues such as D120, E144 and H285 inside the enzymatic active site of RLuc (Figure 1A).

Based on the review of the precedent studies mentioned above, two strategies were adapted in the present study for the synthesis of new CTZ derivatives, which include, (i) introduction of (*p*-hydroxy)-phenyl group in the C-6 position is alkylated (Suppl. Figure 1C-D) to avoid steric hindrance between the luciferin and amino acid residues in the active site; (ii) introduction of hydrophobic moiety into the substrates to improve the cell membrane permeability, which results in the enhancement of BL signals. Totally, 18 CTZ derivatives were newly synthesized and named as “Bottle Blue (BBlue)”, in which mostly the C-6 position was modified (Suppl. Figure 1 C- E).

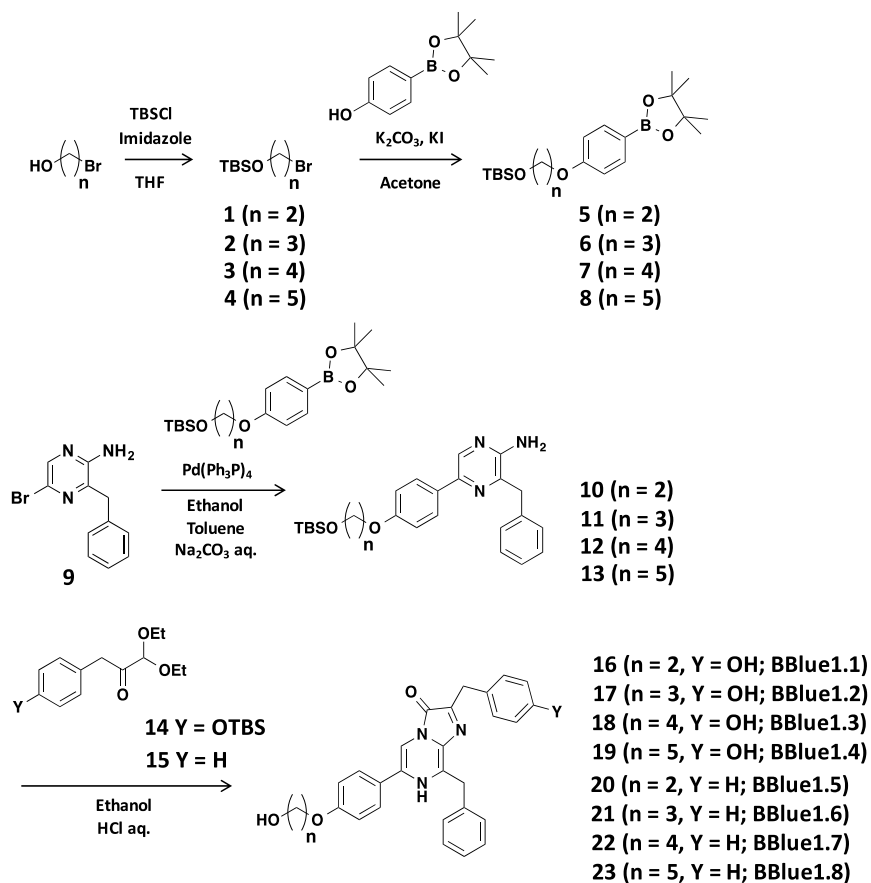
To begin with, the size effect of the C-6 substituent on enzymatic property was investigated. A series of Bottle Blue substrates (Suppl. Figure 1C; group 1) having a different length of straight alkyl linker chains at the C-6 position were synthesized. The series of BBlue1 is characterized as the hydroxyl group terminal at the C-6 position.

The corresponding BL property of the C-6 substituents was determined. The results show that the CTZ derivative with 3-hydroxy propoxy substitution at the C-6 position of the CTZ backbone (Suppl. Figure 1C: BBlue1.2) emits strong BL (Figure 1(D) and Suppl. Figure 2). Thus, we further introduced a series of other functional groups (e.g. methoxy or methyl group) to the C-6 position, which is substituting the alkyl linker chains with three methylene unit length (Suppl. Figure 1E). Because it is known that the electron donating group contributes to the quantum yield (QY) in the imidazopyrazinone backbone [5], we further synthesized a new series of CTZ derivatives that carries electron donating groups (EDG; e.g., methoxy or methyl group) at the C-6 substitution (Suppl. Figures 1C; Group 3).

2. Synthesis

General

All reagents and solvents for organic synthesis were purchased from commercial suppliers (Tokyo Kasei, Aldrich Chemical, Wako Pure Chemicals) and were used without further purification (Analytical grades of >99% purity). All moisture-sensitive reactions were carried out under an atmosphere of argon. The composition of mixed solvents is given by the volume ratio (*v/v*). ¹H-NMR and ¹³C-NMR spectra were recorded on an ECA-500 (JEOL Ltd.) spectrophotometer at room temperature. The measurements for ¹H-NMR was performed at 500 MHz. The measurement of ¹³C-NMR was performed at 125 MHz. All chemical shifts are relative to an internal standard of tetramethylsilane ($\delta = 0.0$ ppm) or solvent residual peaks (CDCl₃: $\delta = 7.26$ ppm, CD₃OD: $\delta = 3.31$ ppm for ¹H; CDCl₃: $\delta = 77.16$ ppm, CD₃OD: $\delta = 49.00$ ppm for ¹³C), and coupling constants are given in Hz. Flash chromatography separation was conducted using a YFLC-AI-560 chromatograph (Yamazen Co. Ltd.). HPLC purification was performed on a reverse-phase column, Intersil ODS-3 (30 × 50 mm) (GL Sciences Inc.), fitted on an LC-918 recycling preparative HPLC system (Japan Analytical Industry Co. Ltd.). High-resolution MS spectra (HR-MS) were recorded on a Waters LCT premier XE with MeOH as the eluent.



Synthetic scheme for Bottle Blue series 1 (BBlue1)

(Compound **1-4**, **9**, **14-15** were synthesized based on previously reported procedures¹⁻⁴)

***tert*-Butyldimethyl(2-(4-(4,4,5,5-tetramethyl-1,3,2-dioxaborolan-2yl)phenoxy)ethoxy)silane (**5**)**

4-(4,4,5,5-Tetramethyl-1,3,2-dioxaborolan-2-yl)phenol (500.0 mg, 2.2 mmol, 1 eq.) and K_2CO_3 (410.0 mg, 2.9 mmol, 1.3 eq.) were dissolved in acetone (20 ml) and stirred at room temperature. (2-Bromoethoxy)(*tert*-butyl)dimethylsilane (**1**) (812.0 mg, 3.4 mmol, 1.5 eq.) and potassium iodide (20.0 mg, 0.1 mmol, 0.05 eq.) were dissolved in acetone (20 ml) and added into the reaction mixture and stirred for 24 hours at 70 °C. After cooling to room temperature, the solution was extracted with ethyl acetate, and the clear organic phase was washed with water and brine, dried over Na_2SO_4 and evaporated. The resulting residue was purified by flash chromatography (silica gel, eluent composition: n-hexane / ethyl acetate = 80/20), affording

tert-butyldimethyl(2-(4-(4,4,5,5-tetramethyl-1,3,2-dioxaborolan-2-yl)phenoxy)ethoxy)silane (**5**) as a white solid end product (307 mg, 36%).

¹H-NMR (500 MHz, CD₃OD): δ (ppm) = 7.73 (d, J = 8.5 Hz, 2H), 6.89 (d, J = 8.5 Hz, 2H), 4.05 (t, J = 5.1 Hz, 2H), 3.97 (t, J = 5.4 Hz, 2H), 1.33(m, 12H), 0.90 (s, 9H), 0.09 (s, 6H). ¹³C-NMR (125 MHz, CDCl₃): δ (ppm) = -5.05, 18.54, 24.99, 26.05, 62.07, 69.18, 83.66, 114.02, 136.61, 161.64. HR-MS: calcd for C₂₀H₃₅BO₄Si: 379.2476 [M+H]⁺, found: m/z 379.2477.

***tert*-Butyldimethyl(3-(4-(4,4,5,5-tetramethyl-1,3,2-dioxaborolan-2-yl)phenoxy)propoxy)silane (6)**

4-(4,4,5,5-Tetramethyl-1,3,2-dioxaborolan-2-yl)phenol (500.0 mg, 2.2 mmol, 1 eq.) and K₂CO₃ (410.0 mg, 2.9 mmol, 1.3 eq.) were dissolved in acetone (20 ml) and stirred at room temperature. (3-Bromopropoxy)(*tert*-butyl)dimethylsilane (**2**) (690.0 mg, 2.7 mmol, 1.2 eq.) and potassium iodide (20.0 mg, 0.1 mmol, 0.05 eq.) were dissolved in acetone (20 ml) and added into the reaction mixture and stirred for 13 hours at 70 °C. After cooling to room temperature, the solution was extracted with ethyl acetate, and the clear organic phase was washed with water and brine, dried over Na₂SO₄ and evaporated. The resulting residue was purified by flash chromatography (silica gel, eluent composition: n-hexane / ethyl acetate = 80/20), affording *tert*-butyldimethyl(3-(4-(4,4,5,5-tetramethyl-1,3,2-dioxaborolan-2-yl)phenoxy)propoxy)silane (**6**) as a white solid product (489.3 mg, 63%)

¹H-NMR (500 MHz, CD₃OD): δ (ppm) = 7.73 (d, J = 8.5 Hz, 2H), 6.89 (d, J = 8.5 Hz, 2H), 4.08 (t, J = 6.3 Hz, 2H), 3.79 (t, J = 6.3 Hz, 2H), 1.97 (m, 2H), 1.32 (s, 12H), 0.88 (s, 9H), 0.03 (s, 6H). ¹³C-NMR (125 MHz, CDCl₃): δ (ppm) = -5.24, 18.45, 25.00, 26.05, 32.45, 59.57, 64.33, 83.67, 113.97, 136.60, 161.79. HR-MS:

calcd for C₂₁H₃₇BO₄Si: 393.2632 [M+H]⁺, found: *m/z* 393.2609.

***tert*-Butyldimethyl(4-(4-(4,4,5,5-tetramethyl-1,3,2-dioxaborolan-2-yl)phenoxy)butoxy)silane (7)**

4-(4,4,5,5-Tetramethyl-1,3,2-dioxaborolan-2-yl)phenol (500.0 mg, 2.2 mmol, 1 eq.) and K₂CO₃ (410.0 mg, 2.9 mmol, 1.3 eq.) were dissolved in acetone (20 ml) and stirred at room temperature. (4-Bromobutoxy)(*tert*-butyl)dimethylsilane (**3**) (721.6 mg, 2.7 mmol, 1.2 eq.) and potassium iodide (20.0 mg, 0.1 mmol, 0.05 eq.) were dissolved in acetone (20 ml) and added into the reaction mixture and stirred for 13 hours at 70 °C. After cooling to room temperature, the solution was extracted with ethyl acetate, and the clear organic phase was washed with water and brine, dried over Na₂SO₄ and evaporated. The resulting residue was purified by flash chromatography (silica gel, eluent composition: n-hexane / ethyl acetate = 80/20), affording *tert*-butyldimethyl(4-(4-(4,4,5,5-tetramethyl-1,3,2-dioxaborolan-2-yl)phenoxy)butoxy)silane (**7**) as a white solid end product (881 mg, 95%)

¹H-NMR (500 MHz, CD₃OD): δ (ppm) = 7.73 (d, *J* = 7.4 Hz, 2H), 6.87 (d, *J* = 7.4 Hz, 2H), 4.00 (t, *J* = 6.0 Hz, 2H), 3.68-3.63 (m, 2H), 1.86-1.81 (m, 2H), 1.70-1.65 (m, 2H), 1.32 (s, 12H), 0.89 (s, 9H), 0.05 (s, 6H). ¹³C-NMR (125 MHz, CDCl₃): δ (ppm) = -5.16, 18.46, 24.98, 25.97, 26.09, 29.44, 62.91, 67.70, 83.63, 113.95, 136.60, 161.81. HR-MS: calcd for C₂₂H₃₉BO₄Si: 407.2789 [M+H]⁺, found: *m/z* 407.2779.

***tert*-Butyldimethyl((5-(4-(4,4,5,5-tetramethyl-1,3,2-dioxaborolan-2-yl)phenoxy)pentyl)oxy)silane (8)**

4-(4,4,5,5-Tetramethyl-1,3,2-dioxaborolan-2-yl)phenol (500.0 mg, 2.2 mmol, 1 eq.) and K₂CO₃ (410.0 mg, 2.9 mmol, 1.3 eq.) were dissolved in acetone (20 ml) and stirred at room temperature.

((5-Bromopentyl)oxy)(*tert*-butyl)dimethylsilane (**4**) (759.5 mg, 2.7 mmol, 1.2 eq.) and potassium iodide (20.0 mg, 0.1 mmol, 0.05 eq.) were dissolved in acetone (20 ml) and added into the reaction mixture and stirred for 7 hours at 70 °C. After cooling to room temperature, the solution was extracted with ethyl acetate, and the clear organic phase was washed with water and brine, dried over Na₂SO₄ and evaporated. The resulting residue was purified by flash chromatography (silica gel, eluent composition: n-hexane / ethyl acetate = 90/10 to 80/20), affording *tert*-butyldimethyl((5-(4-(4,4,5,5-tetramethyl-1,3,2-dioxaborolan-2-yl)phenoxy)pentyl)oxy)silane (**8**) as a white solid product (916 mg, 96%)

¹H-NMR (500 MHz, CD₃OD): δ (ppm) = 7.73 (d, J = 8.5 Hz, 2H), 6.87 (d, J = 8.5 Hz, 2H), 3.98 (t, J = 6.5 Hz, 2H), 3.64-3.60 (m, 2H), 1.81-1.78 (m, 2H), 1.59-1.48 (m, 4H), 1.33 (s, 12H), 0.89 (s, 9H), 0.04 (s, 6H). ¹³C-NMR (125 MHz, CDCl₃): δ (ppm) = -5.13, 18.50, 22.47, 24.99, 26.11, 29.13, 32.66, 63.15, 67.79, 83.64, 113.97, 136.61, 161.84. HR-MS: calcd for C₂₃H₄₁BO₄Si: 421.2945 [M+H]⁺, found: m/z 421.2927.

3-Benzyl-5-(4-(2-((*tert*-butyldimethylsilyl)oxy)ethoxy)phenyl)pyrazin-2-amine (10)

3-Benzyl-5-bromopyrazine-2-amine (**9**) (150 mg, 0.56 mmol, 1 eq.) and *tert*-butyldimethyl(2-(4-(4,4,5,5-tetramethyl-1,3,2-dioxaborolan-2-yl)phenoxy)ethoxy)silane (**5**) (307 mg, 0.81 mmol, 1.4 eq.) were dissolved in toluene (15 ml) and stirred at room temperature. Ethanol (3 ml) and 1 M Na₂CO₃ aq. (4.5 ml) were added into the reaction mixture. After vacuum deaeration, a catalytic amount of tetrakis(triphenylphosphine)palladium(0) was added into the solution and the mixture was deaerated again and stirred for 12 hours at 100 °C. After cooling to room temperature, the solution was filtered through a Celite pad to remove the palladium catalyst. The solution was

extracted with ethyl acetate, and the brown organic phase was washed with water and brine, dried over Na₂SO₄ and evaporated. The resulting residue was purified by flash chromatography (silica gel, eluent composition: n-hexane / ethyl acetate = 80/20 to 70/30), affording 3-benzyl-5-(4-(2-((*tert*-butyldimethylsilyl)oxy)ethoxy)phenyl)pyrazin-2-amine (**10**) as a yellow solid product (225 mg, 92%).

¹H-NMR (500 MHz, CDCl₃): δ (ppm) = 8.33 (s, 1H), 7.86 (d, *J* = 8.5 Hz, 2H), 7.33-7.24 (m, 5H), 6.99 (d, *J* = 8.5 Hz, 2H), 4.33 (s, 2H), 4.17 (s, 2H), 4.09 (t, *J* = 5.1 Hz, 2H), 4.00 (t, *J* = 5.1 Hz, 2H), 0.92 (s, 12H), 0.11 (s, 6H). ¹³C-NMR (125 MHz, CDCl₃): δ (ppm) = -5.02, 18.56, 26.07, 41.40, 62.13, 69.52, 115.00, 127.11, 127.15, 128.70, 129.10, 130.14, 136.99, 140.58, 142.77, 151.38, 159.26. HR-MS: calcd for C₂₅H₃₃N₃O₂Si: 436.2420 [M+H]⁺, found: *m/z* 436.2426.

3-Benzyl-5-(4-(3-((*tert*-butyldimethylsilyl)oxy)propoxy)phenyl)pyrazin-2-amine (11)

3-Benzyl-5-bromopyrazine-2-amine (**9**) (308 mg, 1.16 mmol, 1 eq.) and *tert*-butyldimethyl(3-(4-(4,4,5,5-tetramethyl-1,3,2-dioxaborolan-2-yl)phenoxy)propoxy)silane (**6**) (702.29 mg, 1.85 mmol, 1.6 eq.) were dissolved in toluene (15 ml) and stirred at room temperature. Ethanol (3 ml) and 1 M Na₂CO₃ aq. (4.5 ml) were added into the reaction mixture. After vacuum deaeration, a catalytic amount of tetrakis(triphenylphosphine)palladium(0) was added into the solution and the mixture was deaerated again and stirred for 18 hours at 100 °C. After cooling to room temperature, the solution was filtered through a Celite pad to remove the palladium catalyst. The solution was extracted with ethyl acetate, and the brown organic phase was washed with water and brine, dried over Na₂SO₄ and evaporated. The resulting residue was purified by flash chromatography (silica gel, eluent composition: n-hexane / ethyl acetate = 80/20 to 70/30), affording 3-benzyl-5-(4-(3-((*tert*-butyldimethylsilyl)oxy)propoxy)phenyl)pyrazin-2-amine (**11**) as a

yellow solid product (478.9 mg, 91%).

¹H-NMR (500 MHz, CDCl₃): δ (ppm) = 8.33 (s, 1H), 7.86 (d, *J* = 8.5 Hz, 2H), 7.33-7.25 (m, 5H), 6.98 (d, *J* = 8.5 Hz, 2H), 4.34 (s, 2H), 4.17 (s, 2H), 4.11 (t, *J* = 6.3 Hz, 2H), 3.82 (t, *J* = 5.7 Hz, 2H), 2.00 (quin, *J* = 6.0 Hz, 2H), 0.89 (s, 12H), 0.05 (s, 6H). ¹³C-NMR (125 MHz, CDCl₃): δ (ppm) = -5.21, 18.47, 26.07, 32.50, 41.42, 59.60, 64.67, 114.93, 127.11, 127.15, 128.71, 129.10, 129.93, 137.00, 140.58, 142.86, 151.34, 159.40. HR-MS: calcd for C₂₆H₃₅N₃O₂Si: 450.2577 [M+H]⁺, found: *m/z* 450.2557.

3-Benzyl-5-(4-(4-((*tert*-butyldimethylsilyl)oxy)butoxy)phenyl)pyrazin-2-amine (12)

3-Benzyl-5-bromopyrazine-2-amine (**9**) (180 mg, 0.68 mmol, 1 eq.) and *tert*-butyldimethyl(4-(4-(4,4,5,5-tetramethyl-1,3,2-dioxaborolan-2-yl)phenoxy)butoxy)silane (**7**) (443 mg, 1.09 mmol, 1.6 eq.) were dissolved in toluene (10 ml) and stirred at room temperature. Ethanol (2 ml) and 1 M Na₂CO₃ aq. (3 ml) were added into the reaction mixture. After vacuum deaeration, a catalytic amount of tetrakis(triphenylphosphine)palladium(0) was added into the solution and the mixture was deaerated again and stirred for 15 hours at 100 °C. After cooling to room temperature, the solution was filtered through a Celite pad to remove the palladium catalyst. The solution was extracted with ethyl acetate, and the brown organic phase was washed with water and brine, dried over Na₂SO₄ and evaporated. The resulting residue was purified by flash chromatography (silica gel, eluent composition: n-hexane / ethyl acetate = 80/20 to 67/33), affording 3-benzyl-5-(4-(4-((*tert*-butyldimethylsilyl)oxy)butoxy)phenyl)pyrazin-2-amine (**12**) as a yellow solid product (303.5 mg, 96%).

¹H-NMR (500 MHz, CDCl₃): δ (ppm) = 8.32 (s, 1H), 7.86 (d, *J* = 8.8 Hz, 2H), 7.30-7.25 (m, 5H), 6.97 (d, *J* = 8.5 Hz, 2H), 4.34 (s, 2H), 4.17 (s, 2H), 4.03 (t, *J* = 6.5 Hz, 2H), 3.69 (t, *J* = 6.3 Hz, 2H),

1.89-1.84 (m, 2H), 1.73-1.69 (m, 2H), 0.90 (s, 12H), 0.06 (s, 6H). ^{13}C -NMR (125 MHz, CDCl_3): δ (ppm) = -5.13, 18.49, 26.02, 26.11, 29.48, 41.42, 62.95, 68.04, 114.94, 127.12, 127.16, 128.71, 129.11, 129.94, 136.99, 140.58, 142.87, 151.34, 159.42. HR-MS: calcd for $\text{C}_{27}\text{H}_{37}\text{N}_3\text{O}_2\text{Si}$: 467.2733 $[\text{M}+\text{H}]^+$, found: m/z 464.2724.

3-Benzyl-5-(4-((5-((*tert*-butyldimethylsilyl)oxy)pentyl)oxy)phenyl)pyrazin-2-amine (13)

3-Benzyl-5-bromopyrazine-2-amine (**9**) (180 mg, 0.68 mmol, 1 eq.) and *tert*-butyldimethyl((5-(4-(4,4,5,5-tetramethyl-1,3,2-dioxaborolan-2-yl)phenoxy)pentyl)oxy)silane (**8**) (458 mg, 1.09 mmol, 1.6 eq.) were dissolved in toluene (10 ml) and stirred at room temperature. Ethanol (2 ml) and 1 M Na_2CO_3 aq. (3 ml) were added into the reaction mixture. After vacuum deaeration, a catalytic amount of tetrakis(triphenylphosphine)palladium(0) was added into the solution and the mixture was deaerated again and stirred for 12 hours at 100 °C. After cooling to room temperature, the solution was filtered through a Celite pad to remove the palladium catalyst. The solution was extracted with ethyl acetate, and the brown organic phase was washed with water and brine, dried over Na_2SO_4 and evaporated. The resulting residue was purified by flash chromatography (silica gel, eluent composition: n-hexane / ethyl acetate = 80/20 to 67/33), affording 3-benzyl-5-(4-((5-((*tert*-butyldimethylsilyl)oxy)pentyl)oxy)phenyl)pyrazin-2-amine (**13**) as a yellow solid product (253 mg, 52%).

^1H -NMR (500 MHz, CDCl_3): δ (ppm) = 8.32 (s, 1H), 7.86 (d, J = 8.5 Hz, 2H), 7.30-7.25 (m, 5H), 6.97 (d, J = 8.8 Hz, 2H), 4.34 (s, 2H), 4.17 (s, 2H), 4.01 (t, J = 6.5 Hz, 2H), 3.64 (t, J = 6.3 Hz, 2H), 1.84-1.81 (m, 2H), 1.61-1.57 (m, 2H), 1.54-1.51 (m, 2H), 0.90 (s, 12H), 0.06 (s, 6H). ^{13}C -NMR (125 MHz, CDCl_3): δ (ppm) = -5.11, 18.51, 22.51, 26.13, 29.20, 32.70, 41.42, 63.17, 68.13, 114.95, 127.12, 128.61, 128.71, 129.10, 129.93, 136.98, 140.58, 142.87, 151.34, 159.45. (the signal for one

carbon could not be assigned due to broadening) HR-MS: calcd for C₂₈H₃₉N₃O₂Si: 478.2890 [M+H]⁺, found: *m/z* 478.2876.

8-Benzyl-2-(4-hydroxybenzyl)-6-(4-(2-hydroxyethoxy)phenyl)imidazole[1,2-*a*]pyrazin-3(7*H*)-one (16) (BBlue1.1)

3-Benzyl-5-(4-(2-((*tert*-butyldimethylsilyl)oxy)ethoxy)phenyl)pyrazin-2-amine (**10**) (30 mg, 0.06 mmol, 1 eq.) and 3-(4-((*tert*-butyldimethylsilyl)oxy)phenyl)-1,1-diethoxypropan-2-one (**14**) (47.9 mg, 0.13 mmol, 2 eq.) were dissolved in ethanol (2.0 ml) and H₂O (0.2 ml) and stirred at room temperature. After vacuum deaeration, the solution was cooled to 0 °C and HCl (0.1 ml) was added under nitrogen flow. Once the solution reached room temperature, it was heated and stirred for 5 hours at 80 °C. The solvent was evaporated under vacuum and the crude compound was purified by semipreparative reversed-phase HPLC (eluent composition: CH₃OH / H₂O = 60/40 with 0.1% formic acid), affording 8-benzyl-2-(4-hydroxybenzyl)-6-(4-(2-hydroxyethoxy)phenyl)imidazo[1,2-*a*]pyrazin-3(7*H*)-one (**16**) as a yellow solid (12.8 mg, 45%).

¹H-NMR (500 MHz, CD₃OD): δ (ppm) = 7.63 (s, 1H), 7.56 (d, *J* = 8.3 Hz, 2H), 7.39-7.21 (m, 5H), 7.15 (d, *J* = 8.3 Hz, 2H), 7.03 (d, *J* = 8.3 Hz, 2H), 6.69 (d, *J* = 8.5 Hz, 2H), 4.39 (s, 2H), 4.08-4.06 (m, 4H), 3.88 (t, *J* = 4.8 Hz, 2H). ¹³C-NMR (125 MHz, CD₃OD, CDCl₃): δ (ppm) = 33.20, 61.60, 70.74, 108.17, 116.07, 116.19, 128.13, 129.30, 129.74, 129.78, 130.78, 138.16, 156.97, 161.57. HR-MS: calcd for C₂₈H₂₅N₃O₄: 468.1923 [M+H]⁺, found: *m/z* 468.1923.

8-Benzyl-2-(4-hydroxybenzyl)-6-(4-(3-hydroxypropoxy)phenyl)imidazo[1,2-*a*]pyrazin-3(7*H*)-one (17) (BBlue1.2)

3-Benzyl-5-(4-(3-((*tert*-butyldimethylsilyl)oxy)propoxy)phenyl)pyrazin-2-amine (**11**) (30 mg, 0.06 mmol, 1 eq.) and 3-(4-((*tert*-butyldimethylsilyl)oxy)phenyl)-1,1-diethoxypropan-2-one (**14**) (48.2 mg, 0.13 mmol, 2 eq.) were dissolved in ethanol (2.0 ml) and H₂O (0.2 ml) and stirred at room temperature. After vacuum deaeration, the solution was cooled to 0 °C and HCl (0.1 ml) was added under nitrogen flow. Once the solution reached room temperature, it was heated and stirred for 5.5 hours at 80 °C. The solvent was evaporated under vacuum and the crude compound was purified by semipreparative reversed-phase HPLC (eluent composition: CH₃OH / H₂O = 60/40 with 0.1% formic acid), affording 8-benzyl-2-(4-hydroxybenzyl)-6-(4-(3-hydroxypropoxy)phenyl)imidazo[1,2-*a*]pyrazin-3(*7H*)-one (**17**) as a yellow solid (6.55 mg, 20%).

¹H-NMR (500 MHz, CD₃OD): δ (ppm) = 7.61 (s, 1H), 7.54 (d, *J* = 8.0 Hz, 2H), 7.38-7.20 (m, 5H), 7.14 (d, *J* = 8.5 Hz, 2H), 7.00 (d, *J* = 8.8 Hz, 2H), 6.69 (d, *J* = 8.5 Hz, 2H), 4.39 (s, 2H), 4.10 (t, *J* = 6.3 Hz, 2H), 4.06 (s, 2H), 3.73 (t, *J* = 6.3 Hz, 2H), 1.98 (q, *J* = 6.3 Hz, 2H). ¹³C-NMR (125 MHz, CD₃OD, CDCl₃): δ (ppm) = 33.27, 59.44, 65.90, 108.10, 115.99, 116.20, 128.15, 129.27, 129.75, 130.67, 130.79, 138.13, 156.99, 161.65. HR-MS: calcd for C₂₉H₂₇N₃O₄: 482.2080 [M+H]⁺, found: *m/z* 482.2051.

8-Benzyl-2-(4-hydroxybenzyl)-6-(4-(4-hydroxybutoxy)phenyl)imidazo[1,2-*a*]pyrazin-3(*7H*)-one (18**) (BBlue1.3)**

3-Benzyl-5-(4-(4-((*tert*-butyldimethylsilyl)oxy)butoxy)phenyl)pyrazin-2-amine (**12**) (30 mg, 0.06 mmol, 1 eq.) and 3-(4-((*tert*-butyldimethylsilyl)oxy)phenyl)-1,1-diethoxypropan-2-one (**14**) (48.5 mg, 0.13 mmol, 2 eq.) were dissolved in ethanol (2.0 ml) and H₂O (0.2 ml) and stirred at room temperature. After vacuum deaeration, the solution was cooled to 0 °C and HCl (0.1 ml) was added

under nitrogen flow. Once the solution reached room temperature, it was heated and stirred for 7 hours at 80 °C. The solvent was evaporated under vacuum and the crude compound was purified by chromatograph on a ODS plate (eluent composition: MeCN / H₂O = 50/50), affording 8-benzyl-2-(4-hydroxybenzyl)-6-(4-(4-hydroxybutoxy)phenyl)imidazo[1,2-*a*]pyrazin-3(7*H*)-one (**18**) as a yellow solid (6.96 mg, 20%).

¹H-NMR (500 MHz, CD₃OD): δ (ppm) = 7.61 (s, 1H), 7.54 (d, *J* = 8.3 Hz, 2H), 7.38-7.21 (m, 5H), 7.14 (d, *J* = 8.3 Hz, 2H), 6.98 (d, *J* = 8.3 Hz, 2H), 6.68 (d, *J* = 8.3 Hz, 2H), 4.39 (s, 2H), 4.06 (s, 2H), 4.02 (t, *J* = 6.3 Hz, 2H), 3.62 (t, *J* = 6.3 Hz, 2H), 1.86-1.82 (m, 2H), 1.73-1.69 (m, 2H). ¹³C-NMR (125 MHz, CD₃OD, CDCl₃): δ (ppm) = 26.86, 30.17, 33.24, 35.21, 62.61, 69.00, 108.10, 115.97, 116.19, 128.13, 129.25, 129.74, 129.77, 130.71, 130.78, 138.16, 156.97, 161.65. HR-MS: calcd for C₃₀H₂₉N₃O₄: 496.2236 [M+H]⁺, found: *m/z* 496.2214.

8-Benzyl-2-(4-hydroxybenzyl)-6-(4-((5-hydroxypentyl)oxy)phenyl)imidazo[1,2-*a*]pyrazin-3(7*H*)-one (19**) (BBlue1.4)**

3-Benzyl-5-(4-((5-((*tert*-butyldimethylsilyl)oxy)pentyl)oxy)phenyl)pyrazin-2-amine (**13**) (34.5 mg, 0.07 mmol, 1 eq.) and 3-(4-((*tert*-butyldimethylsilyl)oxy)phenyl)-1,1-diethoxypropan-2-one (**14**) (55.8 mg, 0.15 mmol, 2 eq.) were dissolved in ethanol (2.0 ml) and H₂O (0.2 ml) and stirred at room temperature. After vacuum deaeration, the solution was cooled to 0 °C and HCl (0.1 ml) was added under nitrogen flow. Once the solution reached room temperature, it was heated and stirred for 5 hours at 80 °C. The solvent was evaporated under vacuum and the crude compound was purified by chromatograph on a ODS plate (eluent composition: CH₃OH / H₂O = 50/50), affording 8-benzyl-2-(4-hydroxybenzyl)-6-(4-((5-hydroxypentyl)oxy)phenyl)imidazo[1,2-*a*]pyrazin-3(7*H*)-one (**19**) as a yellow solid (8.77 mg, 21%).

¹H-NMR (500 MHz, CD₃OD): δ (ppm) = 7.61 (s, 1H), 7.53 (d, J = 8.5 Hz, 2H), 7.38-7.14 (m, 5H), 7.15 (d, J = 8.5 Hz, 2H), 6.98 (d, J = 8.8 Hz, 2H), 6.69 (d, J = 8.5 Hz, 2H), 4.39 (s, 2H), 4.06 (s, 2H), 4.00 (t, J = 6.5 Hz, 2H), 3.57 (t, J = 6.3 Hz, 2H), 1.80 (m, 2H), 1.61-1.52 (m, 6H). ¹³C-NMR (125 MHz, CD₃OD, CDCl₃): δ (ppm) = 23.52, 30.14, 33.21, 33.36, 62.82, 69.09, 108.14, 115.95, 116.18, 128.09, 129.23, 129.39, 129.71, 129.78, 130.78, 138.24, 156.95, 161.65. HR-MS: calcd for C₃₁H₃₁N₃O₄: 510.2393 [M+H]⁺, found: m/z 510.2376.

2,8-Dibenzyl-6-(4-(2-hydroxyethoxy)phenyl)imidazo[1,2-*a*]pyrazin-3(7*H*)-one (20) (BBlue1.5)

3-Benzyl-5-(4-(2-((*tert*-butyldimethylsilyl)oxy)ethoxy)phenyl)pyrazin-2-amine (**10**) (71.3 mg, 0.16 mmol, 1 eq.) and 1,1-diethoxy-3-phenylpropan-2-one (**15**) (72.7 mg, 0.32 mmol, 2 eq.) were dissolved in ethanol (4.0 ml) and H₂O (0.4 ml) and stirred at room temperature. After vacuum deaeration, the solution was cooled to 0 °C and HCl (0.2 ml) was added under nitrogen flow. Once the solution reached room temperature, it was heated and stirred for 14 hours at 80 °C. The solvent was evaporated under vacuum and the crude compound was purified by chromatograph on a silica gel plate (eluent composition: CH₃OH / CH₂Cl₂ = 1/10), affording 2,8-dibenzyl-6-(4-(2-hydroxyethoxy)phenyl)imidazo[1,2-*a*]pyrazin-3(7*H*)-one (**20**) as a yellow solid (17.9 mg, 24%).

¹H-NMR (500 MHz, CD₃OD): δ (ppm) = 7.69 (s, 1H), 7.51 (d, J = 7.7 Hz, 2H), 7.37 (d, J = 7.7 Hz, 2H), 7.29-7.11 (m, 7H), 6.97 (d, J = 8.5 Hz, 2H), 4.38 (s, 2H), 4.13 (s, 2H), 4.04 (t, J = 4.5 Hz, 2H), 3.87 (t, J = 5.1 Hz, 2H). ¹³C-NMR (125 MHz, CD₃OD, CDCl₃): δ (ppm) = 33.78, 33.36, 35.39, 61.56, 70.72, 108.51, 116.02, 126.15, 127.44, 127.85, 128.21, 129.27, 129.48, 129.76, 129.81, 132.36, 137.87, 139.71, 161.61. HR-MS: calcd for C₂₈H₂₅N₃O₃: 452.1974 [M+H]⁺, found: m/z 452.1968.

2,8-Dibenzyl-6-(4-(3-hydroxypropoxy)phenyl)imidazo[1,2-*a*]pyrazin-3(7*H*)-one (21) (BBlue1.6)

3-Benzyl-5-(4-(3-((*tert*-butyldimethylsilyl)oxy)propoxy)phenyl)pyrazin-2-amine (**11**) (20 mg, 0.04 mmol, 1 eq.) and 1,1-diethoxy-3-phenylpropan-2-one (**15**) (19.7 mg, 0.08 mmol, 2 eq.) were dissolved in ethanol (2.0 ml) and H₂O (0.2 ml) and stirred at room temperature. After vacuum deaeration, the solution was cooled to 0 °C and HCl (0.1 ml) was added under nitrogen flow. Once the solution reached room temperature, it was heated and stirred for 14 hours at 80 °C. The solvent was evaporated under vacuum and the crude compound was purified by flash chromatography (silica gel, eluent composition: n-hexane / ethyl acetate = 25/75 to ethyl acetate to CH₃OH / ethyl acetate = 10/90 to 20/80), affording 2,8-dibenzyl-6-(4-(3-hydroxypropoxy)phenyl)imidazo[1,2-*a*]pyrazin-3(7*H*)-one (**21**) as a yellow solid (9.38 mg, 45%).

¹H-NMR (500 MHz, CD₃OD): δ (ppm) = 7.60 (s, 1H), 7.52 (s, 2H), 7.38-7.14 (m, 10H), 6.99 (d, J = 8.0 Hz, 2H), 4.39 (s, 2H), 4.16 (s, 2H), 4.09 (t, J = 6.0 Hz, 2H), 3.73 (t, J = 6.3 Hz, 2H), 1.98 (q, J = 6.0 Hz, 2H). ¹³C-NMR (125 MHz, CD₃OD, CDCl₃): δ (ppm) = 18.36, 33.27, 116.00, 128.19, 129.30, 129.48, 129.77, 129.82, 138.04, 139.91, 161.71. HR-MS: calcd for C₂₉H₂₇N₃O₃: 466.2131 [M+H]⁺, found: m/z 466.2112.

2,8-Dibenzyl-6-(4-(4-hydroxybutoxy)phenyl)imidazo[1,2-*a*]pyrazin-3(7*H*)-one (22) (BBlue1.7)

3-Benzyl-5-(4-(4-((*tert*-butyldimethylsilyl)oxy)butoxy)phenyl)pyrazin-2-amine (**12**) (30 mg, 0.06 mmol, 1 eq.) and 1,1-diethoxy-3-phenylpropan-2-one (**15**) (30.6 mg, 0.13 mmol, 2 eq.) were dissolved in ethanol (2.0 ml) and H₂O (0.2 ml) and stirred at room temperature. After vacuum deaeration, the solution was cooled to 0 °C and HCl (0.1 ml) was added under nitrogen flow. Once the

solution reached room temperature, it was heated and stirred for 13.5 hours at 80 °C. The solvent was evaporated under vacuum and the crude compound was purified by chromatograph on a silica gel plate (eluent composition: CH₃OH / ethyl acetate = 1/20), affording 2,8-dibenzyl-6-(4-(4-hydroxybutoxy)phenyl)imidazo[1,2-*a*]pyrazin-3(7*H*)-one (**22**) as a yellow solid (7.73 mg, 20%).

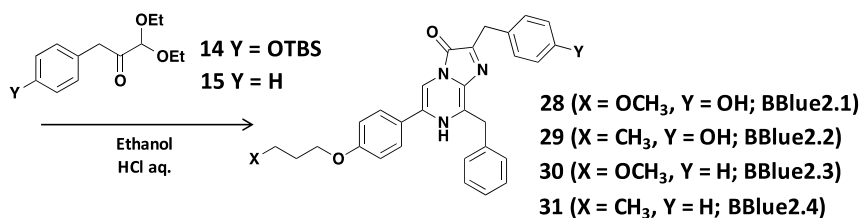
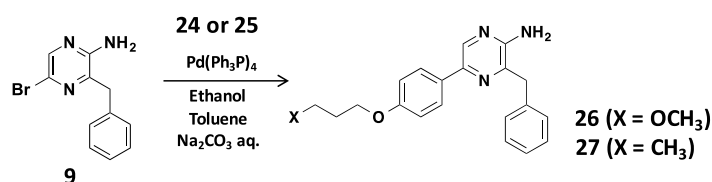
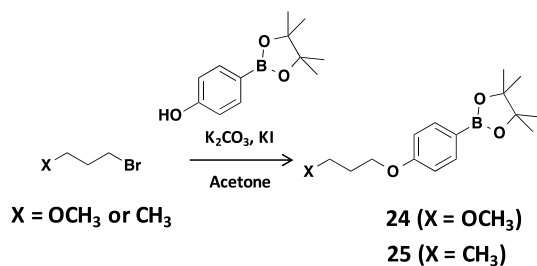
¹H-NMR (500 MHz, CD₃OD): δ (ppm) = 7.61 (s, 1H), 7.51 (s, 2H), 7.38-7.14 (m, 10H), 6.97 (d, *J* = 7.1 Hz, 2H), 4.38 (s, 2H), 4.15 (s, 2H), 4.02 (t, *J* = 6.0 Hz, 2H), 3.61 (t, *J* = 6.3 Hz, 2H), 1.87-1.82 (m, 2H), 1.72-1.67 (m, 2H). ¹³C-NMR (125 MHz, CD₃OD, CDCl₃): δ (ppm) = 26.86, 30.17, 62.60, 69.01, 108.20, 115.98, 127.39, 128.19, 129.29, 129.48, 129.77, 129.82, 138.03, 139.91, 161.71. HR-MS: calcd for C₃₀H₂₉N₃O₃: 480.2287 [M+H]⁺, found: *m/z* 480.2265.

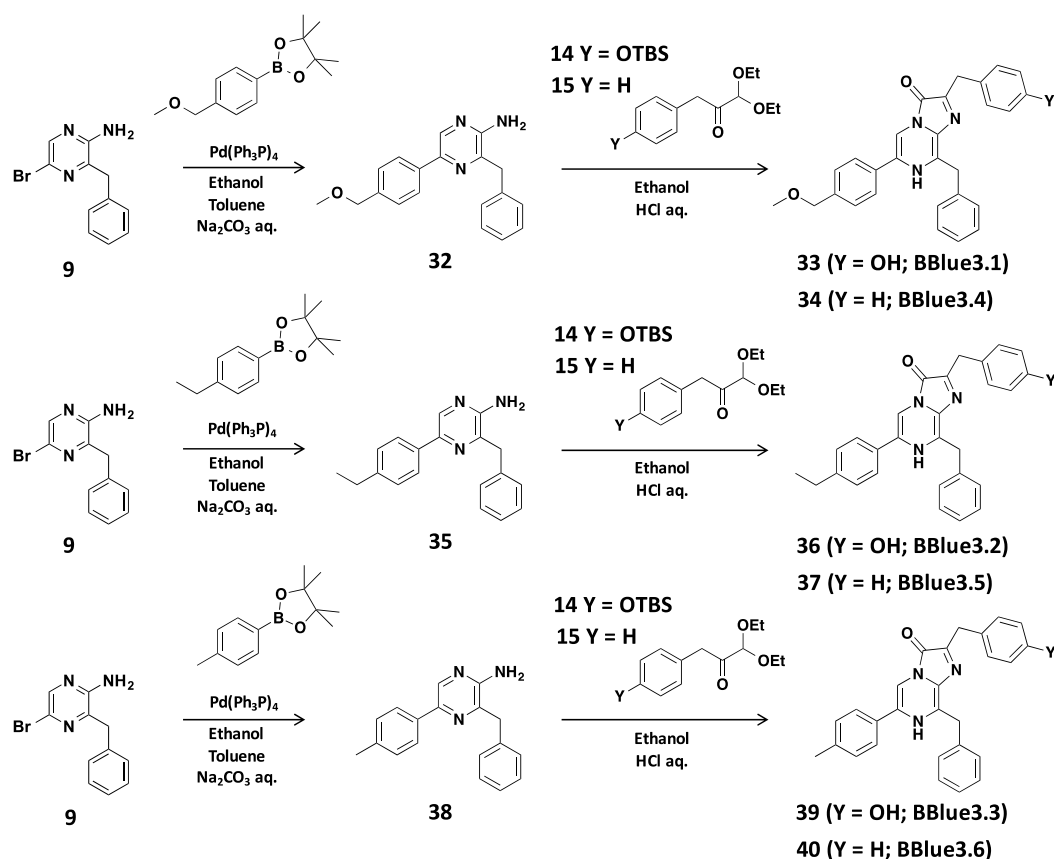
2,8-Dibenzyl-6-(4-((5-hydroxypentyl)phenyl)imidazo[1,2-*a*]pyrazin-3(7*H*)-one (23) (BBlue1.8)

3-Benzyl-5-(4-((5-((*tert*-butyldimethylsilyl)oxy)pentyl)oxy)phenyl)pyrazin-2-amine (**13**) (30.0 mg, 0.06 mmol, 1 eq.) and 1,1-diethoxy-3-phenylpropan-2-one (**15**) (30.4 mg, 0.13 mmol, 2 eq.) were dissolved in ethanol (2.0 ml) and H₂O (0.2 ml) and stirred at room temperature. After vacuum deaeration, the solution was cooled to 0 °C and HCl (0.1 ml) was added under nitrogen flow. Once the solution reached room temperature, it was heated and stirred for 13.5 hours at 80 °C. The solvent was evaporated under vacuum and the crude compound was purified by chromatograph on a silica gel plate (eluent composition: CH₃OH / CH₂Cl₂ = 1/10), affording 2,8-dibenzyl-6-(4-((5-hydroxypentyl)phenyl)imidazo[1,2-*a*]pyrazin-3(7*H*)-one (**23**) as a yellow solid (5.81 mg, 14%).

¹H-NMR (500 MHz, CD₃OD): δ (ppm) = 7.62 (s, 1H), 7.54 (d, *J* = 7.1 Hz, 2H), 7.39-7.15 (m, 10H), 6.99 (d, *J* = 8.0 Hz, 2H), 4.39 (s, 2H), 4.16 (s, 2H), 4.01 (t, *J* = 6.0 Hz, 2H), 3.57 (t, *J* = 6.5 Hz, 2H),

1.83-1.79 (m, 2H), 1.62-1.52 (m, 4H). $^{13}\text{C-NMR}$ (125 MHz, CD_3OD , CDCl_3): δ (ppm) = 23.53, 30.14, 33.36, 62.82, 69.12, 108.19, 116.00, 127.39, 128.19, 129.31, 129.48, 129.56, 129.77, 129.83, 131.37, 138.05, 139.93, 161.78. HR-MS: calcd for $\text{C}_{31}\text{H}_{31}\text{N}_3\text{O}_3$: 494.2444 $[\text{M}+\text{H}]^+$, found: m/z 494.2415.





Synthetic scheme for Bottle Blue series 2 and 3

(compound **24** and **25** were synthesized based on reported procedures ⁴)

3-Benzyl-5-(4-(3-methoxypropoxy)phenyl)pyrazin-2-amine (**26**)

3-Benzyl-5-bromopyrazin-2-amine (**9**) (100 mg, 0.3 mmol, 1 eq.) and 2-(4-(3-methoxypropoxy)phenyl)-4,4,5,5-tetramethyl-1,3,2-dioxaborolane (**24**) (176.9 mg, 0.6 mmol, 2.0 eq.) were dissolved in toluene (6 ml) and stirred at room temperature. Ethanol (1 ml) and 1 M Na₂CO₃ aq. (2 ml) were added into the reaction mixture. After vacuum deaeration, a catalytic amount of tetrakis(triphenylphosphine)palladium(0) was added into the solution and the mixture was deaerated again and stirred for 12 hours at 100 °C. After cooling to room temperature, the solution was filtered through a Celite pad to remove the palladium catalyst. The solution was extracted with ethyl acetate, and the brown organic phase was washed with water and brine, dried over Na₂SO₄ and evaporated. The resulting residue was purified by flash chromatography (silica gel, eluent

composition: n-hexane / ethyl acetate = 67/33 to 50/50), affording 3-benzyl-5-(4-(3-methoxypropoxy)phenyl)pyrazin-2-amine (**26**) as a yellow solid (127.3 mg, 96%).

¹H-NMR (500 MHz, CDCl₃): δ (ppm) = 8.32 (s, 1H), 7.86 (d, J = 8.3 Hz, 2H), 7.33-7.26 (m, 5H), 6.98 (d, J = 8.8 Hz, 2H), 4.34 (s, 2H), 4.17 (s, 2H), 4.11 (t, J = 6.0 Hz, 2H), 3.58 (t, J = 6.3 Hz, 2H), 1.33 (m, 12H), 0.90 (s, 9H), 0.09 (s, 6H). ¹³C-NMR (125 MHz, CDCl₃): δ (ppm) = 29.75, 41.38, 58.87, 65.06, 69.36, 114.95, 127.11, 128.58, 128.70, 129.08, 130.04, 132.26, 136.97, 140.57, 142.77, 151.36, 139.31.

3-Benzyl-5-(4-butoxyphenyl)pyrazin-2-amine (**27**)

3-Benzyl-5-bromopyrazine-2-amine (**9**) (100 mg, 0.3 mmol, 1 eq.) and 2-(4-butoxyphenyl)-4,4,5,5-tetramethyl-1,3,2-dioxaborolane (**25**) (167 mg, 0.4 mmol, 1.6 eq.) were dissolved in toluene (6 ml) and stirred at room temperature. Ethanol (1 ml) and 1 M Na₂CO₃ aq. (2 ml) were added into the reaction mixture. After vacuum deaeration, a catalytic amount of tetrakis(triphenylphosphine)palladium(0) was added into the solution and the mixture was deaerated again and stirred for 13 hours at 100 °C. After cooling to room temperature, the solution was filtered through a Celite pad to remove the palladium catalyst. The solution was extracted with ethyl acetate, and the brown organic phase was washed with water and brine, dried over Na₂SO₄ and evaporated. The resulting residue was purified by flash chromatography (silica gel, eluent composition: n-hexane / ethyl acetate = 80/20 to 67/33), affording 3-benzyl-5-(4-butoxyphenyl)pyrazin-2-amine (**27**) as a yellow solid (121.6 mg, 96%).

¹H-NMR (500 MHz, CDCl₃): δ (ppm) = 8.33 (s, 1H), 7.86 (d, J = 8.8 Hz, 2H), 7.33-7.23 (m, 5H), 6.98 (d, J = 8.8 Hz, 2H), 4.34 (s, 2H), 4.17 (s, 2H), 4.01 (t, J = 6.5 Hz, 2H), 1.79 (m, 2H), 1.52 (m, 2H), 0.99 (t, J = 7.4 Hz, 2H). ¹³C-NMR (125 MHz, CDCl₃): δ (ppm) = 14.02, 19.39, 31.45, 41.42,

67.92, 114.95, 127.12, 127.15, 128.71, 129.10, 129.89, 136.99, 140.58, 142.87, 151.34, 159.48.

8-Benzyl-6-(4-butoxyphenyl)-6-(4-(3-methoxypropoxy)phenyl)imidazo[1,2-*a*]pyrazin-3(7*H*)-one (28) (BBlue2.1)

3-Benzyl-5-(4-(3-methoxypropoxy)phenyl)pyrazin-2-amine (**26**) (35.0 mg, 0.1 mmol, 1 eq.) and 3-(4-((tert-butyldimethylsilyl)oxy)phenyl)-1,1-diethoxypropan-2-one (**14**) (70.5 mg, 0.2 mmol, 2 eq.) were dissolved in ethanol (2.0 ml) and H₂O (0.2 ml) and stirred at room temperature. After vacuum deaeration, the solution was cooled to 0 °C and HCl (0.1 ml) was added under nitrogen flow. Once the solution reached room temperature, it was heated and stirred for 6 hours at 80 °C. The solvent was evaporated under vacuum and the crude compound was purified by chromatography (silica gel, eluent composition: CH₃OH / CH₂Cl₂ = 1/20), affording 8-benzyl-6-(4-butoxyphenyl)-6-(4-(3-methoxypropoxy)phenyl)imidazo[1,2-*a*]pyrazin-3(7*H*)-one (**28**) as a yellow solid (18.2 mg, 52%).

¹H-NMR (500 MHz, CD₃OD): δ (ppm) = 7.61 (s, 1H), 7.47 (d, *J* = 5.1 Hz, 2H), 7.36 (d, *J* = 7.4 Hz, 2H), 7.27-7.12 (m, 5H), 6.92 (d, *J* = 6.3 Hz, 2H), 6.67 (d, *J* = 7.1 Hz, 2H), 4.36 (s, 2H), 4.03 (s, 4H), 3.53 (t, *J* = 6.3 Hz, 2H), 3.33 (s, 3H), 2.02-1.97 (m, 2H). ¹³C-NMR (125 MHz, CD₃OD): δ (ppm) = 30.50, 33.19, 35.16, 58.91, 66.04, 70.29, 108.15, 115.66, 115.91, 116.21, 127.84, 128.14, 129.20, 129.55, 129.74, 129.77, 130.63, 130.79, 138.08, 156.99, 161.53.

8-Benzyl-6-(4-butoxyphenyl)-2-(4-hydroxybenzyl)imidazo[1,2-*a*]pyrazin-3(7*H*)-one (29) (BBlue2.2)

3-Benzyl-5-(4-butoxyphenyl)pyrazin-2-amine (**27**) (30.0 mg, 0.08 mmol, 1 eq.) and 3-(4-((tert-butyldimethylsilyl)oxy)phenyl)-1,1-diethoxypropan-2-one (**14**) (63.4 mg, 0.17 mmol, 2

eq.) were dissolved in ethanol (2.0 ml) and H₂O (0.2 ml) and stirred at room temperature. After vacuum deaeration, the solution was cooled to 0 °C and HCl (0.1 ml) was added under nitrogen flow. Once the solution reached room temperature, it was heated and stirred for 6 hours at 80 °C. The solvent was evaporated under vacuum and the crude compound was purified by chromatography (silica gel, eluent composition: CH₃OH / CH₂Cl₂ = 1/20), affording 8-benzyl-6-(4-butoxyphenyl)-2-(4-hydroxybenzyl)imidazo[1,2-*a*]pyrazin-3(7*H*)-one (**29**) as a yellow solid (12.8 mg, 30%).

¹H-NMR (500 MHz, CD₃OD, CDCl₃): δ (ppm) = 7.57 (s, 1H), 7.51 (d, *J* = 8.0 Hz, 2H), 7.41 (d, *J* = 8.3 Hz, 2H), 7.31-7.18 (m, 5H), 6.98 (d, *J* = 8.5 Hz, 2H), 6.72 (d, *J* = 8.5 Hz, 2H), 4.39 (s, 2H), 4.10 (s, 2H), 4.02 (t, *J* = 6.3 Hz, 2H), 1.81-1.75 (m, 2H), 1.54-1.49 (m, 2H), 1.00 (t, *J* = 7.4 Hz, 3H).
¹³C-NMR (125 MHz, CD₃OD, CDCl₃): δ (ppm) = 14.09, 19.87, 31.95, 68.55, 107.73, 115.64, 115.90, 127.83, 128.78, 129.39, 129.43, 130.39, 137.39, 156.22, 161.15.

2,8-Dibenzyl-6-(4-(3-methoxypropoxy)phenyl)imidazo[1,2-*a*]pyrazin-3(7*H*)-one (30) (BBlue2.3)

3-Benzyl-5-(4-(3-methoxypropoxy)phenyl)pyrazin-2-amine (**26**) (30.0 mg, 0.08 mmol, 1 eq.) and 1,1-diethoxy-3-phenylpropan-2-one (**14**) (38.0 mg, 0.17 mmol, 2 eq.) were dissolved in ethanol (2.0 ml) and H₂O (0.2 ml) and stirred at room temperature. After vacuum deaeration, the solution was cooled to 0 °C and HCl (0.1 ml) was added under nitrogen flow. Once the solution reached room temperature, it was heated and stirred for 16 hours at 80 °C. The solvent was evaporated under vacuum and the crude compound was purified by chromatography (silica gel, eluent composition: CH₃OH / CH₂Cl₂ = 1/20), affording 2,8-dibenzyl-6-(4-(3-methoxypropoxy)phenyl)imidazo[1,2-*a*]pyrazin-3(7*H*)-one (**30**) as a yellow solid (22.6 mg, 55%).

¹H-NMR (500 MHz, CD₃OD, CDCl₃): δ (ppm) = 7.54 (s, 1H), 7.47 (d, *J* = 8.5 Hz, 2H), 7.38 (d, *J* = 7.4 Hz, 2H), 7.32 (d, *J* = 7.4 Hz, 2H), 7.27-7.12 (m, 6H), 6.93 (d, *J* = 8.8 Hz, 2H), 4.36 (s, 2H), 4.15 (s, 2H), 4.03 (t, *J* = 6.3 Hz, 2H), 3.54 (t, *J* = 6.0 Hz, 2H), 3.33 (s, 3H), 2.03-1.98 (m, 2H). ¹³C-NMR (125 MHz, CD₃OD, CDCl₃): δ (ppm) = 30.36, 34.06, 34.96, 58.91, 65.90, 70.06, 108.09, 115.83, 125.75, 127.24, 127.72, 128.06, 129.32, 129.61, 129.66, 129.69, 137.76, 139.65, 152.49, 161.35.

2,8-Dibenzyl-6-(4-butoxyphenyl)imidazo[1,2-*a*]pyrazin-3(7*H*)-one (31) (BBlue2.4)

3-Benzyl-5-(4-butoxyphenyl)pyrazin-2-amine (**27**) (32.7 mg, 0.09 mmol, 1 eq.) and 1,1-diethoxy-3-phenylpropan-2-one (**15**) (43.7 mg, 0.19 mmol, 2 eq.) were dissolved in ethanol (2.0 ml) and H₂O (0.2 ml) and stirred at room temperature. After vacuum deaeration, the solution was cooled to 0 °C and HCl (0.1 ml) was added under nitrogen flow. Once the solution reached room temperature, it was heated and stirred for 21 hours at 80 °C. The solvent was evaporated under vacuum and the crude compound was purified by chromatography (silica gel, eluent composition: CH₃OH / CH₂Cl₂ = 1/20), affording 2,8-dibenzyl-6-(4-butoxyphenyl)imidazo[1,2-*a*]pyrazin-3(7*H*)-one (**31**) as a yellow solid (27.4 mg, 60%).

¹H-NMR (500 MHz, CD₃OD, CDCl₃): δ (ppm) = 7.45 (s, 1H), 7.48 (d, *J* = 8.3 Hz, 2H), 7.39 (d, *J* = 7.3 Hz, 2H), 7.33 (d, *J* = 7.4 Hz, 2H), 7.28-7.13 (m, 6H), 6.94 (d, *J* = 8.8 Hz, 2H), 4.38 (s, 2H), 4.16 (s, 2H), 3.96 (t, *J* = 6.5 Hz, 2H), 1.78-1.72 (m, 2H), 1.52-1.47 (m, 2H), 0.97 (t, *J* = 7.4 Hz, 3H). ¹³C-NMR (125 MHz, CD₃OD, CDCl₃): δ (ppm) = 14.15, 20.08, 32.18, 34.08, 34.84, 68.71, 107.99, 115.79, 127.19, 128.03, 129.01, 129.27, 129.58, 129.61, 129.65, 137.69, 139.55, 161.46.

3-Benzyl-5-(4-(methoxymethyl)phenyl)pyrazin-2-amine (32)

3-Benzyl-5-bromopyrazine-2-amine (**9**) (166.0 mg, 0.6 mmol, 1 eq.) and

2-(4-(methoxymethyl)phenyl)-4,4,5,5-tetramethyl-1,3,2-dioxaborolane (249.5 mg, 1.0 mmol, 1.6 eq.) were dissolved in toluene (12 ml) and stirred at room temperature. Ethanol (2 ml) and 1 M Na₂CO₃ aq. (3 ml) were added into the reaction mixture. After vacuum deaeration, a catalytic amount of tetrakis(triphenylphosphine)palladium(0) was added into the solution and the mixture was deaerated again and stirred for 13 hours at 100 °C. After cooling to room temperature, the solution was filtered through a Celite pad to remove the palladium catalyst. The solution was extracted with ethyl acetate, and the brown organic phase was washed with water and brine, dried over Na₂SO₄ and evaporated. The resulting residue was purified by flash chromatography (silica gel, eluent composition: n-hexane / ethyl acetate = 67/33 to 50/50), affording 3-benzyl-5-(4-(methoxymethyl)phenyl)pyrazin-2-amine (**32**) as a yellow solid (169.5 mg, 88%).

¹H-NMR (500 MHz, CDCl₃): δ (ppm) = 8.39 (s, 1H), 7.93 (d, *J* = 8.3 Hz, 2H), 7.42 (d, *J* = 8.3 Hz, 2H), 7.43-7.25 (m, 5H), 4.51 (s, 2H), 4.42 (s, 2H), 4.19 (s, 2H), 3.4 (s, 2H). ¹³C-NMR (125 MHz, CDCl₃): δ (ppm) = 41.42, 58.18, 74.53, 76.90, 77.16, 77.41, 125.91, 127.21, 128.33, 128.71, 129.13, 136.85, 137.65, 138.17, 140.74, 142.51, 151.88.

8-Benzyl-2-(4-hydroxybenzyl)-6-(4-(methoxymethyl)phenyl)imidazo[1,2-*a*]pyrazin-3(7*H*)-one
(33) (BBlue3.1)

3-Benzyl-5-(4-(methoxymethyl)phenyl)pyrazin-2-amine (**32**) (30.0 mg, 0.09 mmol, 1 eq.) and 3-(4-((tert-butyldimethylsilyl)oxy)phenyl)-1,1-diethoxypropan-2-one (**14**) (69.2 mg, 0.19 mmol, 2 eq.) were dissolved in ethanol (2.0 ml) and H₂O (0.2 ml) and stirred at room temperature. After vacuum deaeration, the solution was cooled to 0 °C and HCl (0.1 ml) was added under nitrogen flow. Once the solution reached room temperature, it was heated and stirred for 4 hours at 80 °C. The solvent was evaporated under vacuum and the crude compound was purified by chromatography

(silica gel, eluent composition: CH₃OH / CH₂Cl₂ = 1/20), affording 8-benzyl-2-(4-hydroxybenzyl)-6-(4-(methoxymethyl)phenyl)imidazo[1,2-*a*]pyrazin-3(7*H*)-one (**33**) as a yellow solid (13.8 mg, 31%).

¹H-NMR (500 MHz, CD₃OD): δ (ppm) = 7.70 (s, 1H), 7.59 (d, *J* = 7.4 Hz, 2H), 7.39-7.18 (m, 7H), 7.14 (d, *J* = 8.3 Hz, 2H), 6.68 (d, *J* = 8.5 Hz, 2H), 4.44 (s, 2H), 4.38 (s, 2H), 4.05 (s, 2H), 3.31-3.30 (m, 3H). ¹³C-NMR (125 MHz, CD₃OD): δ (ppm) = 33.22, 35.34, 58.47, 74.94, 108.97, 116.22, 127.80, 128.16, 129.15, 129.27, 129.75, 129.79, 129.89, 130.57, 130.78, 138.05, 141.20, 157.02.

2,8-Dibenzyl-6-(4-(methoxymethyl)phenyl)imidazo[1,2-*a*]pyrazin-3(7*H*)-one (34) (BBlue3.4)

3-Benzyl-5-(4-(methoxymethyl)phenyl)pyrazin-2-amine (**32**) (30.4 mg, 0.09 mmol, 1 eq.) and 1,1-diethoxy-3-phenylpropan-2-one (**15**) (44.2 mg, 0.19 mmol, 2 eq.) were dissolved in ethanol (2.0 ml) and H₂O (0.2 ml) and stirred at room temperature. After vacuum deaeration, the solution was cooled to 0 °C and HCl (0.1 ml) was added under nitrogen flow. Once the solution reached room temperature, it was heated and stirred for 4 hours at 80 °C. The solvent was evaporated under vacuum and the crude compound was purified by chromatography (silica gel, eluent composition: CH₃OH / CH₂Cl₂ = 1/20), affording 2,8-dibenzyl-6-(4-(methoxymethyl)phenyl)imidazo[1,2-*a*]pyrazin-3(7*H*)-one (**34**) (29.35 mg, 68%).

¹H-NMR (500 MHz, CD₃OD, CDCl₃): δ (ppm) = 8.32 (s, 1H), 7.83 (d, *J* = 6.0 Hz, 2H), 7.45-7.23 (m, 11H), 4.52 (s, 2H), 4.49 (s, 2H), 4.27 (s, 2H), 3.40 (m, 3H). ¹³C-NMR (125 MHz, CD₃OD, CDCl₃): δ (ppm) = 31.67, 37.69, 58.55, 74.86, 110.68, 127.81, 127.84, 128.22, 129.19, 129.41, 129.62, 129.66, 130.01, 133.74, 136.89, 138.30, 141.41, 146.26.

3-Benzyl-5-(4-ethylphenyl)pyrazin-2-amine (35)

3-Benzyl-5-bromopyrazine-2-amine (**9**) (100 mg, 0.3 mmol, 1 eq.) and 2-(4-ethylphenyl)-4,4,5,5-tetramethyl-1,3,2-dioxaborolane (140.4 mg, 0.6 mmol, 1.6 eq.) were dissolved in toluene (6 ml) and stirred at room temperature. Ethanol (1 ml) and 1 M Na₂CO₃ aq. (2 ml) were added into the reaction mixture. After vacuum deaeration, a catalytic amount of tetrakis(triphenylphosphine)palladium(0) was added into the solution and the mixture was deaerated again and stirred for 12 hours at 100 °C. After cooling to room temperature, the solution was filtered through a Celite pad to remove the palladium catalyst. The solution was extracted with ethyl acetate, and the brown organic phase was washed with water and brine, dried over Na₂SO₄ and evaporated. The resulting residue was purified by flash chromatography (silica gel, eluent composition: n-hexane / ethyl acetate = 70/30), affording 3-benzyl-5-(4-ethylphenyl)pyrazin-2-amine (**35**) as a yellow solid (100.4 mg, 91%).

¹H-NMR (500 MHz, CDCl₃): δ (ppm) = 8.37 (s, 1H), 7.86 (d, *J* = 8.0 Hz, 2H), 7.33-7.25 (m, 7H), 4.37 (s, 2H), 4.18 (s, 2H), 2.70 (t, *J* = 7.4 Hz, 2H), 1.28-1.25 (m, 3H). ¹³C-NMR (125 MHz, CDCl₃): δ (ppm) = 15.78, 28.79, 41.42, 76.90, 77.16, 77.41, 125.91, 127.16, 128.48, 128.71, 129.11, 134.87, 136.95, 137.44, 140.67, 142.96, 144.47, 151.66.

8-Benzyl-6-(4-ethylphenyl)-2-(4-hydroxybenzyl)imidazo[1,2-*a*]pyrazin-3(7*H*)-one (**36**)

(BBlue3.2)

3-Benzyl-5-(4-ethylphenyl)pyrazin-2-amine (**35**) (30.0 mg, 0.1 mmol, 1 eq.) and 3-(4-((tert-butyldimethylsilyl)oxy)phenyl)-1,1-diethoxypropan-2-one (**14**) (72.6 mg, 0.20 mmol, 2 eq.) were dissolved in ethanol (2.0 ml) and H₂O (0.2 ml) and stirred at room temperature. After vacuum deaeration, the solution was cooled to 0 °C and HCl (0.1 ml) was added under nitrogen flow. Once the solution reached room temperature, it was heated and stirred for 21 hours at 80 °C. The

solvent was evaporated under vacuum and the crude compound was purified by chromatography (silica gel, eluent composition: CH₃OH / CH₂Cl₂ = 1/20), affording 8-benzyl-6-(4-ethylphenyl)-2-(4-hydroxybenzyl)imidazo[1,2-*a*]pyrazin-3(7*H*)-one (**36**) as a yellow solid (9.6 mg, 21%).

¹H-NMR (500 MHz, CD₃OD): δ (ppm) = 7.65 (s, 1H), 7.53 (d, *J* = 7.1 Hz, 2H), 7.38 (d, *J* = 7.7 Hz, 2H), 7.30-7.20 (m, 5H), 7.15 (d, *J* = 8.3 Hz, 2H), 6.69 (d, *J* = 8.3 Hz, 2H), 4.39 (s, 2H), 4.06 (2H), 2.68 (q, *J* = 7.4 Hz, 2H), 1.22 (q, *J* = 7.4 Hz, 3H). ¹³C-NMR (125 MHz, CD₃OD): δ (ppm) = 15.98, 29.58, 33.27, 108.54, 116.21, 127.87, 128.18, 129.58, 129.76, 130.59, 130.80, 138.06, 147.38, 157.01.

2,8-Dibenzyl-6-(4-ethylphenyl)imidazo[1,2-*a*]pyrazin-3(7*H*)-one (37) (BBlue3.5)

3-Benzyl-5-(4-ethylphenyl)pyrazin-2-amine (**35**) (35.7 mg, 0.12 mmol, 1 eq.) and 1,1-diethoxy-3-phenylpropan-2-one (**15**) (54.9 mg, 0.24 mmol, 2 eq.) were dissolved in ethanol (3.0 ml) and H₂O (0.3 ml) and stirred at room temperature. After vacuum deaeration, the solution was cooled to 0 °C and HCl (0.2 ml) was added under nitrogen flow. Once the solution reached room temperature, it was heated and stirred for 14 hours at 80 °C. The solvent was evaporated under vacuum and the crude compound was purified by chromatography (silica gel, eluent composition: CH₃OH / CH₂Cl₂ = 1/20), affording 2,8-dibenzyl-6-(4-ethylphenyl)imidazo[1,2-*a*]pyrazin-3(7*H*)-one (**37**) as a yellow solid (48.85 mg, 94%).

¹H-NMR (500 MHz, CD₃OD, CDCl₃): δ (ppm) = 7.48 (s, 1H), 7.41 (d, *J* = 7.4 Hz, 2H), 7.35 (d, *J* = 7.1 Hz, 2H), 7.30-7.15 (m, 10H), 4.39 (s, 2H), 4.19 (s, 2H), 2.65 (q, *J* = 7.4 Hz, 2H), 1.23 (q, *J* = 7.7 Hz, 3H). ¹³C-NMR (125 MHz, CD₃OD, CDCl₃): δ (ppm) = 15.68, 29.07, 34.00, 34.48, 108.07, 124.81, 126.74 126.85, 127.14, 127.25, 127.72, 128.20, 128.42, 128.70, 128.93, 129.05, 129.24,

129.27, 129.30, 136.42, 137.00, 138.94, 146.65.

3-Benzyl-5-(*p*-tolyl)pyrazin-2-amine (38)

3-Benzyl-5-bromopyrazine-2-amine (**9**) (123.9 mg, 0.4 mmol, 1 eq.) and 4,4,5,5-tetramethyl-2-(*p*-tolyl)-1,3,2-dioxaborolane (102.0 mg, 0.7 mmol, 1.6 eq.) were dissolved in toluene (6 ml) and stirred at room temperature. Ethanol (1 ml) and 1 M Na₂CO₃ aq. (2 ml) were added into the reaction mixture. After vacuum deaeration, a catalytic amount of tetrakis(triphenylphosphine)palladium(0) was added into the solution and the mixture was deaerated again and stirred for 19 hours at 100 °C. After cooling to room temperature, the solution was filtered through a Celite pad to remove the palladium catalyst. The solution was extracted with ethyl acetate, and the brown organic phase was washed with water and brine, dried over Na₂SO₄ and evaporated. The resulting residue was purified by flash chromatography (silica gel, eluent composition: n-hexane / ethyl acetate = 80/20 to 70/30), affording 3-benzyl-5-(*p*-tolyl)pyrazin-2-amine (**38**) as a yellow solid (123.97 mg, 96%).

¹H-NMR (500 MHz, CDCl₃): δ (ppm) = 8.38 (s, 1H), 7.82 (d, *J* = 8.0 Hz, 2H), 7.32-7.23 (m, 7H), 4.53 (s, 2H), 4.17 (s, 2H), 2.39 (s, 3H). ¹³C-NMR (125 MHz, CDCl₃): δ (ppm) = 21.36, 41.34, 125.76, 127.16, 128.68, 129.09, 129.63, 134.50, 136.83, 138.07, 140.92, 142.98, 151.48.

8-Benzyl-2-(4-hydroxybenzyl)-6-(*p*-tolyl)imidazo[1,2-*a*]pyrazin-3(7*H*)-one (39) (BBlue3.3)

3-Benzyl-5-(*p*-tolyl)pyrazin-2-amine (**38**) (32.6 mg, 0.1 mmol, 1 eq.) and 3-(4-((tert-butyldimethylsilyl)oxy)phenyl)-1,1-diethoxypropan-2-one (**14**) (83.6 mg, 0.2 mmol, 2 eq.) were dissolved in ethanol (2.0 ml) and H₂O (0.2 ml) and stirred at room temperature. After vacuum deaeration, the solution was cooled to 0 °C and HCl (0.1 ml) was added under nitrogen flow. Once the

solution reached room temperature, it was heated and stirred for 21 hours at 80 °C. The solvent was evaporated under vacuum and the crude compound was purified by chromatography (silica gel, eluent composition: CH₃OH / CH₂Cl₂ = 1/20 to 1/10), affording 8-benzyl-2-(4-hydroxybenzyl)-6-(*p*-tolyl)imidazo[1,2-*a*]pyrazin-3(7*H*)-one (**39**) as a yellow solid (23.12 mg, 50%).

¹H-NMR (500 MHz, CD₃OD): δ (ppm) = 7.57 (s, 1H), 7.42 (d, *J* = 7.4 Hz, 2H), 7.37 (d, *J* = 7.4 Hz, 2H), 7.27-7.13 (m, 7H), 6.68 (d, *J* = 8.3 Hz, 2H), 4.36 (s, 2H), 4.04 (s, 2H), 2.28 (s, 3H). ¹³C-NMR (125 MHz, CD₃OD): δ (ppm) = 21.24, 33.28, 35.13, 108.51, 116.22, 127.62, 127.80, 128.16, 129.74, 129.77, 130.56, 130.62, 130.80, 138.01, 140.89, 157.00.

2,8-Dibenzyl-6-(*p*-tolyl)imidazo[1,2-*a*]pyrazin-3(7*H*)-one (40) (BBlue3.6)

3-Benzyl-5-(*p*-tolyl)pyrazin-2-amine (**38**) (32.0 mg, 0.1 mmol, 1 eq.) and 1,1-diethoxy-3-phenylpropan-2-one (**15**) (51.6 mg, 0.2 mmol, 2 eq.) were dissolved in ethanol (2.0 ml) and H₂O (0.2 ml) and stirred at room temperature. After vacuum deaeration, the solution was cooled to 0 °C and HCl (0.1 ml) was added under nitrogen flow. Once the solution reached room temperature, it was heated and stirred for 21 hours at 80 °C. The solvent was evaporated under vacuum and the crude compound was purified by chromatography (silica gel, eluent composition: CH₃OH / CH₂Cl₂ = 1/40 to 1/20), affording 2,8-dibenzyl-6-(*p*-tolyl)imidazo[1,2-*a*]pyrazin-3(7*H*)-one (**40**) as a yellow solid (24.08 mg, 54%).

¹H-NMR (500 MHz, CD₃OD, CDCl₃): δ (ppm) = 7.45 (s, 1H), 7.41 (d, *J* = 7.1 Hz, 2H), 7.36 (d, *J* = 7.4 Hz, 2H), 7.31-7.17 (m, 10H), 4.39 (s, 2H), 4.19 (s, 2H), 2.37 (s, 3H). ¹³C-NMR (125 MHz, CD₃OD): δ (ppm) = 21.35, 34.03, 34.35, 108.11, 126.94, 127.16, 127.81, 129.02, 129.34, 129.35, 129.58, 130.30, 137.15, 139.08, 140.43.

3. Chemiluminescence assay

3.1. Materials

All solvents for spectrometry were purchased from Kanto Chemical (Tokyo) of >99% purity. The commercial substrates, Native CTZ (nCTZ), DeepBlueC (DBlueC), Prolume Purple, Prolume Purple 2, Prolume Purple 3, Prolume Purple 4 and Prolume Purple 5, were purchased from NanoLight Technology (Pinetop, AZ, USA). The nCTZ and its derivatives were diluted with ethanol and stored in sealed glass ampules at ~80°C.

3.2. Chemiluminescence assays of CTZ derivatives

In order to obtain the chemiluminescence characteristics, methanol solution of nCTZ or the respective CTZ derivatives (2 mM, 8 μ L) was mixed with DMSO (80 μ L) containing 0.25% (*v/v*) of 1 M aqueous sodium hydroxide in a 200 μ L microtube. The microtube was immediately moved into the chamber of a precision spectrophotometer (AB-1850, ATTO), equipped with a cooled charge-coupled device (CCD) camera which can detect signals of all the emission wavelengths from 400 nm to 800 nm at once. The resulting spectra were taken in a 1 second integration mode. The optical spectra were normalized to percentages (%) for plotting graphs.

3.3. Comment on the chemiluminescence (CL) assay

To discuss the luciferin-luciferase binding chemistry, the chemiluminescence (CL) spectra were determined. Each CL spectrum of the substrates was immediately recorded after addition of an aliquot of DMSO into the substrate tube and summarized in Suppl. Table 1. The results show that all the new CTZ derivatives were brighter than DeepBlueC. This result is not surprising,

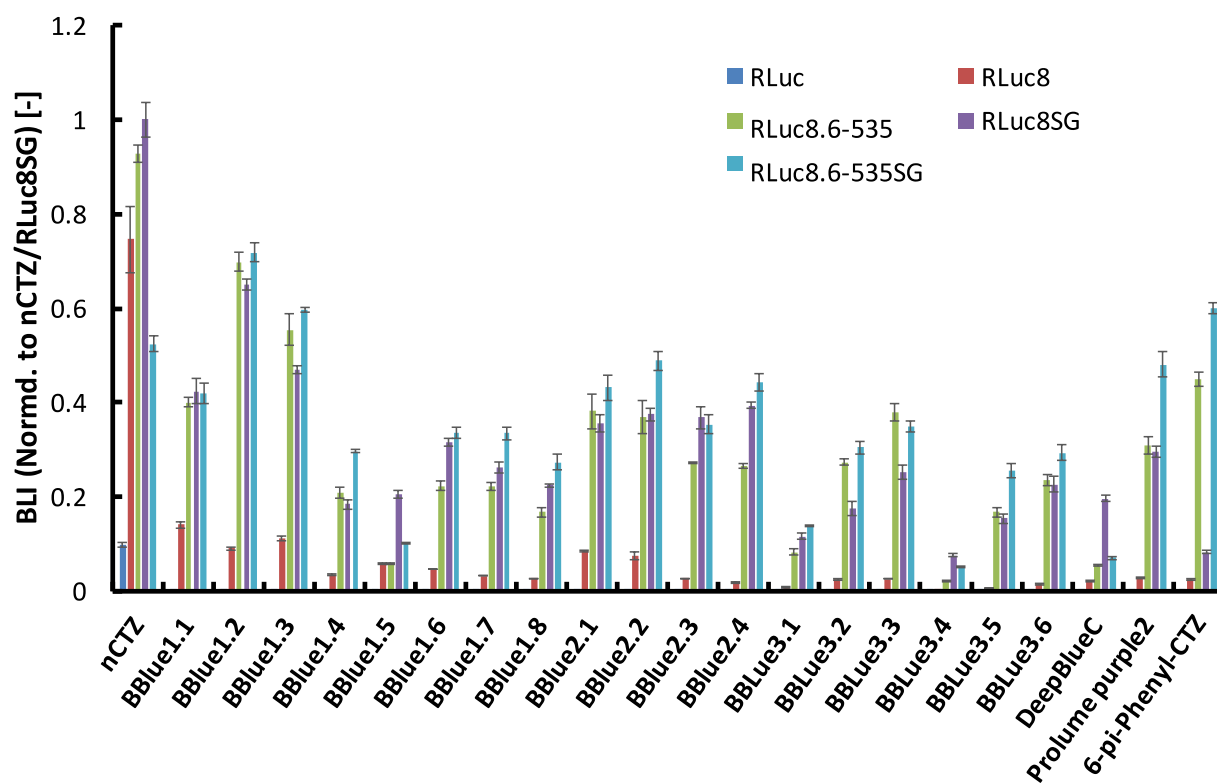
considering the previous study that the EDG at the C-6 of the imidazopyrazinone backbone elevates the fluorescence (FL) quantum yield (QY) [5]. Therefore, the superior light output of the new CTZ derivatives compared to DeepBlueC was attributed to the existence of an electron-donating substituent at the para-position of the C-6 phenyl group of CTZ (Suppl. Figure 1). The spectral peak similarity among new CTZ derivatives indicates that the chemical modification at the C-6 substituent has little influence on the energy gaps between the ground and excitation states of CL, except for 6-*pi*-Phenyl-CTZ. We hypothesized that the red-shifted spectrum of 6-*pi*-Phenyl-CTZ is due to a reduction of the dihedral twisting between the C-6 substituent and the imidazopyrazinone skeleton as discussed previously [1].

Suppl Table 1. Summary of chemiluminescence (CL) characteristics: Initial CL intensities (CLI) and CL spectra in the presence of an aliquot of DMSO solution containing 0.25% (v/v) of 1 M aqueous sodium hydroxide (CL was integrated for 1 s). Under this condition, the CLI of 6-*pi*-Phenyl-CTZ could not be obtained due to its light flux exceeding the maximal detection range. According to CL spectra, the styryl substitution at C-6 position extends its conjugated π -electron system and strongly influences on CL quantum yield (QY). N.D means Not detected

	CL intensity (CLI) (%)	CL spectrum Emission max. [nm]
nCTZ	100	510
BBlue1.1	113	499
BBlue1.2	113	500
BBlue1.3	84.3	499
BBlue1.5	122	499
BBlue1.6	91.4	498
BBlue1.7	105	498

BBlue2.1	98.2	497
BBlue2.2	92.4	493
BBlue2.3	116	499
BBlue2.4	124	501
BBlue3.1	90.1	493
BBlue3.2	125	500
BBlue3.3	110	499
BBlue3.4	104	495
BBlue3.5	92.2	492
BBlue3.6	130	500
DeepBlueC	69.0	489
6-pi-Phenyl-CTZ	N.D.	528

4. Bioluminescence assay



Suppl. Figure 2. Initial BLI from new CTZ derivatives (2 μ L). The BLI was immediately recorded for 1 second after mixing each substrate with 4 μ L of cell lysates containing the designated luciferase (RLuc, RLuc8, RLuc8.6-535, RLuc8SG, or RLuc8.6-535SG).

Suppl Table 2. Substrates initial bioluminescence intensities (BLI) with different *Renilla* luciferase (RLuc) variants [native RLuc (nCTZ), RLuc8, RLuc8.6-535, RLuc8SG and RLuc8.6-535SG; BLI was integrated for the initial 1s]

	RLuc	RLuc8	RLuc8SG	RLuc8.6-535	RLuc8.6-535SG
	BLI (%)	BLI (%)	BLI (%)	BLI (%)	BLI (%)
nCTZ	9.94	74.6	100	92.6	52.4
BBlue1.1	N.D.	13.9	42.4	40.0	41.9
BBlue1.2	0.10	9.03	64.9	69.8	71.7
BBlue1.3	N.D.	10.9	46.9	55.4	59.5
BBlue1.4	N.D.	3.48	18.3	20.9	29.5
BBlue1.5	N.D.	5.75	20.4	5.78	10.1
BBlue1.6	N.D.	4.66	31.4	22.2	33.6
BBlue1.7	N.D.	3.20	26.2	22.2	33.4
BBlue1.8	N.D.	2.67	22.4	16.6	27.3
BBlue2.1	N.D.	8.52	35.5	38.1	43.1
BBlue2.2	N.D.	7.48	37.5	36.7	48.8
BBlue2.3	N.D.	2.72	36.7	27.1	35.3
BBlue2.4	N.D.	1.85	39.3	26.4	44.1
BBlue3.1	N.D.	0.79	11.5	8.29	13.7
BBlue3.2	N.D.	2.49	17.5	27.2	30.4
BBlue3.3	N.D.	2.53	25.0	38.0	35.0
BBlue3.4	N.D.	0.33	7.59	2.01	4.99
BBlue3.5	N.D.	0.58	15.3	16.7	25.5
BBlue3.6	N.D.	1.34	22.6	23.5	29.2
DeepBlueC	N.D.	2.14	19.5	5.37	6.99

Prolume Purple 2	N.D.	2.73	29.6	30.7	48.0
6-pi-Phenyl-CTZ	N.D.	2.60	8.18	45.0	59.9

The term “N.D.” means “not detected” due to low luminescent intensity

4.1. Determination of the initial bioluminescence intensities (BLIs) of the new CTZ derivatives with different variants of *Renilla* luciferase

The initial bioluminescence intensities (BLIs) of all the synthesized CTZ derivatives (2 μ M) were determined with the cell lysates of different variants of *Renilla* luciferase (RLuc, RLuc8, RLuc8.6-535, RLuc8SG and RLuc8.6-535SG). A comparison of the initial BLI (Suppl. Figure 2 and Suppl. Table 2) shows that all the CTZ derivatives with a C-6 modification produced significant level of luminescent signal with different RLuc variants (RLuc8, RLuc8.6-535, RLuc8SG and RLuc8.6-535SG) except RLuc. It should be noted that all the CTZ derivatives emit superior BL with RLuc8.6-535SG, compared to DeepBlueC. Among the CTZ derivatives, the derivative with 3-hydroxypropoxy group (BBlue1.2; Suppl Figure 1 Group (B)) shows the brightest BL emission with RLuc8.6-535SG. Its intensity is ~71 % of that of the nCTZ/RLuc8SG pair.

In order to determine the variation in BLI according to the alkyl linker lengths, we determined the BLI of the CTZ derivatives with a hydroxyl-terminated alkyl linker containing two, three, four or five consecutively chained methylene units (Suppl Figure 1 Group(B)). We compared the substrates with RLuc8.6-535SG. The 4-hydroxybutoxy group-substituted derivative (BBlue1.3) exhibits similar, but slightly decreased BLI, compared to BBlue1.2. BBlue1.4 having the longest alkyl chain linker at the C-6 position of the imidazopyrazinone backbone shows the lowest BL emission among the BBlue 1 series of CTZ derivatives (Suppl Figure 1 Group (B)). Thus, the optimal alkyl chain length at the C-6 position of imidazopyrazinone for high BLI is supposed with a 3-hydroxypropoxy group. It is generally accepted that the bulkiness of the substituent in the luciferin backbone adversely

influences on the BLI. However, in contrast to the expectation, the BBlue1.3/RLuc8.6-535SG pair emitted 1.4-fold brighter BL signal than the BBlue1.1/RLuc8.6-535SG pair, although the side alkyl chain of BBlue1.3 has two methylene units longer than BBlue1.1. This result may be explained as the size at the C-6 position of CTZ is not the only factor involved in the enzymatic reaction, but the appropriate interactions between the C-6 substituent and the amino acid residues located around the substrate binding pocket may contribute for the elevated BLI. Next, the initial BLI of the Group 1 substrates in Suppl Figure 1(C) was compared with the results of Suppl Figure 2.

The results show that the group bearing the hydroxyl group at the C-2 para position (BBlue1.1-1.3) is generally superior to the ones without the hydroxyl group (BBlue1.5–1.8) in the BLI. On the other hand, the hydroxyl group at the C-2 para position has no clear effect in case of Group 2 and Group 3, considering the BLIs of BBlue 2.1–2.2 vs BBlue 2.3–2.4 and the BLIs of BBlue 3.1–3.3 vs BBlue 3.4–3.6. The results may be interpreted as the hydroxyl group at the para position of the C-2 of Group 2 and 3 is not a determinant factor for BLI with RLucs.

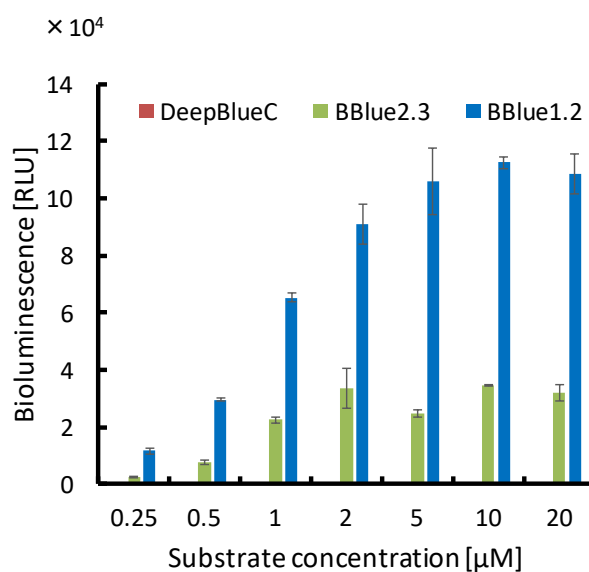
Furthermore, it should be noted that BLI of BBlue1.2 is 1.6- and 1.4-fold higher than those of BBlue2.1 and BBlue2.2, respectively, although their chemical structures are similar to each other except the hydroxyl group at the C-6 position. This result implicates that the hydroxyl group at the para position of the C-6 considerably influences on the interaction with RLucs with the substrate.

Finally, the effect of the EDG (methoxy or methyl group) at the C-6 substituent on BLI was compared with that of the conventional blue-shifted substrate, the DeepBlueC (Suppl Figure 2). BBlue3.6 carrying a methyl group at the C-6 but lacking the hydroxyl group at the C-2 showed nearly 4.1-fold stronger BLI than the chemically resembled CTZ derivative, DeepBlueC, which has no hydroxyl groups at both of the C-2 and C-6 positions, in the presence of RLuc8.6-535SG. Not

only BBlue3.6, but also BBlue3.5 having an ethyl group at the para position of the C-6 phenyl group exerted stronger BLI than DeepBlueC. Although the CL and BL properties of luciferins are not always completely correlated, the dim BLI of DeepBlueC may be attributed to its relatively low CL efficiency (Suppl. Table 1) and poor catalytic proficiency (V_{\max}/K_m) with RLuc8.6-535 variants (Suppl. Table 3). The enzymatic recognition mechanism of nCTZ and BBlue1.2 was further elucidated with RLuc variants; that is a computational docking simulation of luciferin with RLuc8 was conducted using Autodock4.2.6 [6] using a crystal structure (PDB: 2PSJ) of an 8-mutation variant of RLuc (RLuc8) [4] (Suppl. Figure 9 and Suppl. Table 6).

In BL systems, the luminescence kinetic profiles arise from the turn-over rate. As an inhibition effect of the oxidated product (coelenteramide, CTMD), QY should be carefully considered to properly evaluate BLIs. Actually, DeepBlueC showed the brightest emission with RLuc8SG, although the other C-6 CTZ derivatives prefer RLuc8.6-535SG as a catalytic enzyme.

Substrate-dose dependency of BLI with RLuc8.6-535 protein expressed in *E. coli* and column purified



Suppl Figure 3. Substrate-dose dependent BLI of the pure RLuc8.6-535 expressed in *E.coli*. The results show that the BLI reaches an optical plateau in 2 and 5 minutes with BBlue2.3 and BBlue1.2, respectively. DeepBlueC did not show significant BL with purified RLuc8.6-535 reporter protein.

Suppl Table 3. The kinetic constants of all the CTZ derivatives in combination with purified RLuc8.6-535. ^aMichaelis-Menten constant (K_m) and maximum rate (V_{max}) were estimated with the Michaelis-Menten kinetics equation using GraphPad Prism ver. 7. The average values are shown with the standard deviation (\pm SD) from the data of independent assays in triplicate.^cThe “relative quantum yield (QY)” was calculated by dividing the total BLI of CTZs by the total molar number of substrate molecules present in the applied reaction solution, and expressed in the relative values to that of nCTZ. The total BLIs were determined by integrating all the photons after complete consumption of a low concentration of luciferins (0.25 μ M) with an excess amount of RLuc8.6-535.
^cData from our previous study [1].

	Relative initial BLI [-]	K_m^a [μM]	V_{\max}^b [s p^{-1}]	V_{\max}/K_m [$\times 10^3 \text{p s}^{-1} \mu\text{M}^{-1}$]	Relative QY ^c [-]
NCTZ	100	0.69 ± 0.07	(1.11 \pm 0.02) $\times 10^5$	160.8	100
BBlue1.1	43.1	1.31 ± 0.12	(5.54 \pm 0.13) $\times 10^4$	42.29	86
BBlue1.2	75.3	1.00 ± 0.13	(1.25 \pm 0.04) $\times 10^5$	125.00	84
BBlue1.3	59.8	0.92 ± 0.15	(8.26 \pm 0.34) $\times 10^4$	89.78	43
BBlue1.4	22.5	0.42 ± 0.11	(1.86 \pm 0.10) $\times 10^4$	44.28	11
BBlue1.5	6	2.06 ± 0.30	(6.04 \pm 0.26) $\times 10^4$	29.32	30
BBlue1.6	23.9	0.85 ± 0.40	(2.65 \pm 0.56) $\times 10^4$	31.17	22
BBlue1.7	23.9	1.12 ± 0.29	(3.56 \pm 0.24) $\times 10^4$	31.78	7
BBlue1.8	17.9	1.11 ± 0.15	(1.66 \pm 0.06) $\times 10^4$	14.95	5
BBlue2.1	41.1	1.12 ± 0.15	(5.54 \pm 0.20) $\times 10^4$	49.46	34
BBlue2.2	39.6	0.79 ± 0.18	(2.99 \pm 0.19) $\times 10^4$	37.84	6
BBlue2.3	29.2	0.75 ± 0.20	(3.79 \pm 0.24) $\times 10^4$	50.53	23
BBlue2.4	28.5	0.33 ± 0.04	(2.30 \pm 0.11) $\times 10^4$	69.69	77

BBlue3.1	8.9	0.30 ± 0.03	(1.06 ± 0.02) × 10 ⁴	35.33	21
BBlue3.2	29.3	0.41 ± 0.12	(3.10 ± 0.31) × 10 ⁴	75.60	27
BBlue3.3	41.0	1.02 ± 0.21	(4.28 ± 0.42) × 10 ⁴	41.96	12
BBlue3.4	2.1	0.26 ± 0.02	(4.94 ± 0.08) × 10 ³	19.00	2
BBlue3.5	18.0	0.57 ± 0.12	(2.12 ± 0.17) × 10 ⁴	37.19	14
BBlue3.6	25.3	0.92 ± 0.22	(3.88 ± 0.43) × 10 ⁴	42.17	10
DeepBlueC	5.7	0.31 ± 0.009	(3.16 ± 0.04) × 10 ³	10.19	2
Prolume Purple	2				
6-pi-Phenyl-CTZ	33.8 ^e	0.60 ± 0.09	(2.84 ± 0.13) × 10 ⁴	47.33	25

4.2.Determination of the bioluminescence kinetic profile with RLuc8.6-535

To evaluate the detailed BL properties, we determined the kinetic constants of CTZ derivatives with affinity column-purified RLuc8.6-535. The results were summarized in Suppl. Table 3. The K_m values of the CTZ derivatives with a modified C-6 sidechain are in the range of 0.2-2.0 μM with RLuc8.6-535, which includes that of nCTZ ($0.69 \pm 0.07 \mu\text{M}$). The broad range of K_m indicates that the C-6 position of CTZ is a determining factor for the high affinity for luciferase. And the maximum rates, V_{max} , show that BBlue1.2 ($(1.25 \pm 0.04) \times 10^5 \text{ s} \cdot \text{p}^{-1}$) achieves the highest rate, followed by nCTZ ($(1.11 \pm 0.02) \times 10^5 \text{ s} \cdot \text{p}^{-1}$) and BBlue1.3 ($(8.26 \pm 0.34) \times 10^4 \text{ s} \cdot \text{p}^{-1}$), order of

which corresponds with the results obtained by initial BLI measurements.

On the other hand, the K_m and V_{max} values of DeepBlueC are $0.31 \mu\text{M}$ and $((3.16 \pm 0.04) \times 10^3 \text{ s} \cdot \text{p}^{-1})$, respectively. Therefore, DeepBlueC may be considered to have high affinity for RLuc8.6-535, whereas the V_{max} value is relatively low compared to the other CTZ derivatives. For explaining this disaccordance, the V_{max}/K_m value, which is proportional to the k_{cat}/K_m value, and the relative QY values are further discussed below in the view of the catalytic efficiency of RLuc8.6-535.

The comparison of V_{max}/K_m values of nCTZ, BBlue1.2, BBlue1.3 and DeepBlueC reveals that RLuc8.6-535 exhibits a higher catalytic efficiency for nCTZ ($160.8 \times 10^3 \text{ s} \cdot \text{p}^{-1} \cdot \mu\text{M}^{-1}$), followed by BBlue1.2 ($125.0 \times 10^3 \text{ s} \cdot \text{p}^{-1} \cdot \mu\text{M}^{-1}$), BBlue1.3 ($89.7 \times 10^3 \text{ s} \cdot \text{p}^{-1} \cdot \mu\text{M}^{-1}$) and DeepBlueC ($10.1 \times 10^3 \text{ s} \cdot \text{p}^{-1} \cdot \mu\text{M}^{-1}$). In addition, the relative QY values are also in the order of nCTZ, BBlue1.2, BBlue1.3 and DeepBlueC, the order of which corresponds with the V_{max}/K_m values.

Furthermore, the BL-half-life of nCTZ (121 s), BBlue1.2 (101 s) and BBlue1.3 (109 s) is quite longer than DeepBlueC (15 s). Because RLuc shows a flash manner of BL influenced by inhibitory effect of the BL reaction product (CTMD) [7], it is interpreted as the strong BL of BBlue1.2 is contributed by its relative high catalytic turn-over rate and light production efficiency of the substrate in excited state compared to the other CTZ derivatives.

Suppl Table 4. BL spectra with native RLuc, RLuc8, RLuc8.6-535, RLuc8SG, RLuc8.6-535SG and CL spectra under basic condition.

	RLuc8 Peak (nm) [FWHM (nm)]	RLuc8SG Peak (nm) [FWHM (nm)]	RLuc8.6-535 Peak (nm) [FWHM (nm)]	RLuc8.6-535SG Peak (nm) [FWHM (nm)]	CL Peak (nm) [FWHM (nm)]
NCTZ	484 [98]	490 [92]	538 [111]	530 [106]	510 [96]

BBlue1.1	411 [59]	415 [54]	411 [56]	412 [62]	499 [84]
BBlue1.2	414 [60]	412 [53]	415 [56]	415 [51]	500 [85]
BBlue1.3	404 [69]	404 [71]	412 [60]	411 [62]	499 [84]
BBlue1.4	403 [70]	422 [53]	406 [66]	413 [51]	496 [85]
BBlue1.5	413 [65]	405 [70]	407 [68]	405 [69]	499 [86]
BBlue1.6	411 [65]	405 [71]	413 [56]	411 [51]	498 [87]
BBlue1.7	404 [69]	404 [71]	405 [68]	412 [52]	498 [86]
BBlue1.8	403 [70]	406 [71]	406 [68]	414 [49]	492 [87]
BBlue2.1	(418) [44]	412 [65]	412 [59]	412 [59]	497 [83]
BBlue2.2	(413) [46]	412 [65]	412 [60]	412 [62]	493 [87]
BBlue2.3	416 [49]	414 [55]	413 [53]	411 [53]	499 [86]
BBlue2.4	411 [50]	414 [56]	413 [53]	413 [54]	501 [86]
BBlue3.1	(420) [-]	414 [53]	411 [49]	410 [51]	493 [91]
BBlue3.2	(410) [-]	401 [65]	406 [60]	412 [60]	500 [86]
BBlue3.3	415 [44]	410 [52]	413 [51]	412 [50]	499 [89]
BBlue3.4	(393) [-]	412 [56]	406 [53]	412 [50]	495 [96]
BBlue3.5	(402) [-]	414 [52]	411 [50]	411 [50]	492 [91]
BBlue3.6	408 [45]	412 [53]	411 [49]	411 [50]	500 [92]
DeepBlueC™	416 [57]	416 [59]	410 [51]	412 [49]	489 [94]
Prolume Purple 2	ND	ND	ND	ND	ND
6-pi-Phenyl-CTZ	434 [61]	434 [66]	426 [64]	426 [63]	528 [84]

FWHM: full width at half maximum

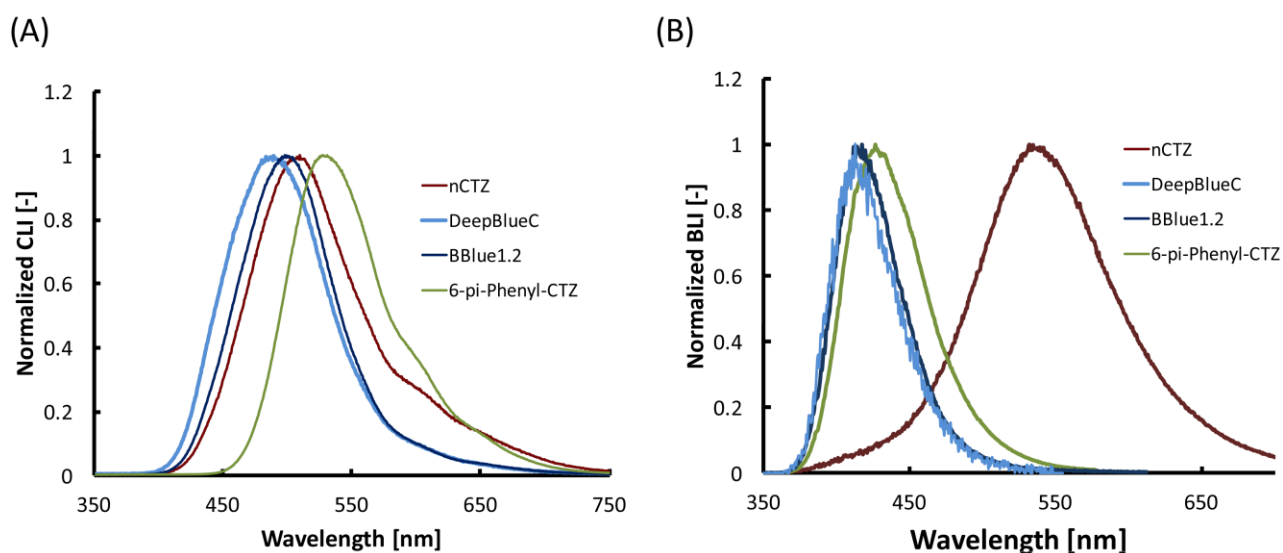
4.3. Determination of the luminescence spectra of CTZ derivatives

The CL and BL spectra of all the CTZs were investigated for discussing the unique optical properties. The spectral characteristics are summarized in Suppl Figure 4 and Suppl. Table 4. The maximal CL emission of C-6 modified CTZ derivatives is located around 500 nm, almost identical to the nCTZ (Suppl. Figure 4A and Suppl. Table 4). The similar emission spectra of nCTZ and the derivatives may be explained as they have the similar energy state gaps among the amide anion species of the substrates in the excited state. And the minor influence of the C-6 substituents in the substrates on the CL spectrum has been described in Suppl. Figure 4A.

It is known that, during the enzymatic reaction, CTZ can form three possible intermediate formations in different protonation states (e.g. neutral species, phenolate anion or pyrazine anion species), which determine the emission color [8] ^[9]. In the BL spectra of the C-6 modified CTZ derivatives with RLuc derivatives, the blue-shifted emission (maximum at 401–426 nm) comes from the only neutral form of the intermediates in the excited state, implying that the C-6 modification prevents the deprotonation of the *p*-hydroxyl group on the C-6 phenyl of the substrate. This precedent view explains why our new CTZ derivatives are bright in the blue region. The results also mean that we successfully developed bright blue-shifted CTZ derivatives, which can be alternatives to DeepBlueC.

In addition, the full width at half maximum (FWHM) values of RLuc mutants with BBlue1.2 and nCTZ are 51 nm and 89 nm, respectively (Suppl. Figure 4B and Suppl. Table 4). The large variance in the FWHM values attributes to the number of light emitters (intermediates) in the transition state: i.e., the broader FWHM of nCTZ is explained by the presence of more light emitters than the new C-6-modified CTZ derivatives. In addition, the comparison of the spectral shapes between BL and

CL, the FWHMs of the CL spectra are generally broad with any C-6 modified CTZ derivatives, suggesting that multiple, stable light emitting species are participated in the excited state (Suppl. Figure 4A and Suppl. Table 4).



Suppl Figure 4. (A) CL spectra of nCTZ and C-6-modified CTZ derivatives (DeepBlueC, BBlue1.2 and 6-pi-Phenyl-CTZ). The spectrum intensities were normalized for comparison. (B) BL spectra of nCTZ and C-6 modified CTZ derivatives (DeepBlueC, BBlue1.2 and 6-pi-Phenyl-CTZ) in combination with RLuc8.6-535SG. The spectrum intensities were normalized for comparison.

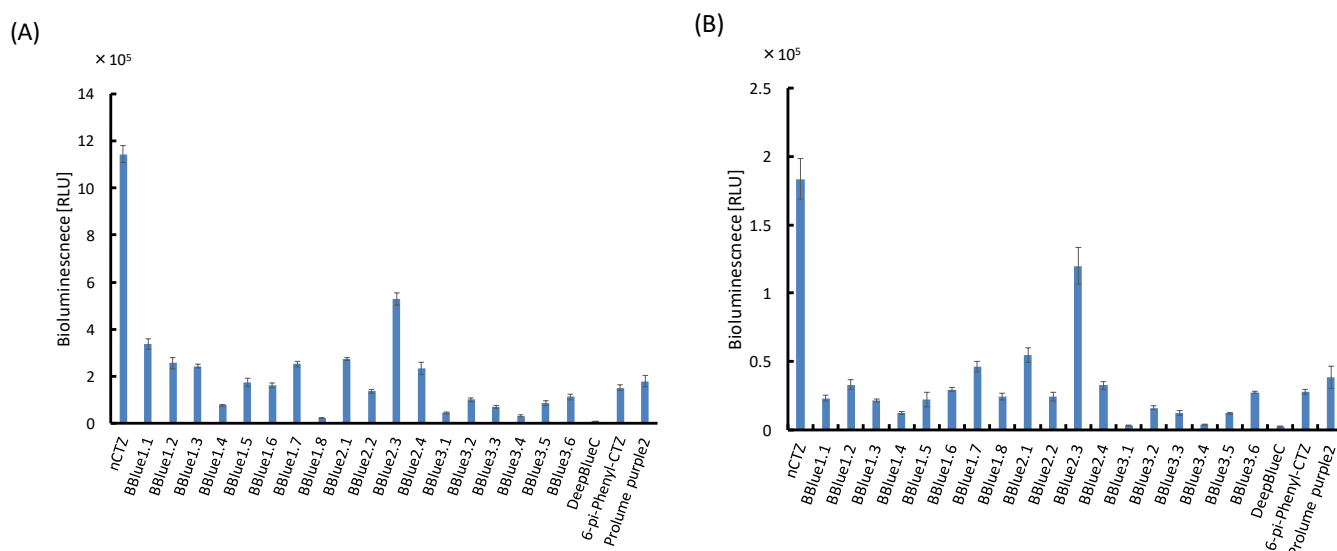
4.4. Determination of bioluminescence intensities (BLI) in living cells

The BLI of all CTZ derivatives were determined in living HeLa or COS-7 cells expressing RLuc8.6-535SG (Suppl. Figure 5).

HeLa cells or COS-7 cells were subcultured in a 96-well black frame optical-bottom microplate (Thermo Scientific) and transiently transfected with pcDNA3.1 (+) plasmids encoding RLuc8.6SG

using a TransIT-LT1 transfection reagent (Takara, Osaka, Japan) and incubated for 24 h to 48 h. After removal of the cell culture medium, the cells were incubated with Hanks' balanced salt solution (HBSS) (100 μ L) and simultaneously treated with HBSS buffer (100 μ L) containing 20 μ M nCTZ or the respective CTZ derivatives (final CTZ concentration: 10 μ M). The plate was immediately set in the dark chamber of the Lumazon FA image analyzer (Nippon Roper), and the corresponding luminescence intensities were determined throughout 30 min.

The live cell experiments show that the highest BLI is obtained with nCTZ, and followed by BBlue2.3, the tendency of which is similar in both COS-7 and HeLa cells. The BLI order was different from the results of the cell lysates. This discrepancy may be explained with the role of the plasma membranes, which can be a barrier for less membrane-permeability of CTZ derivatives. Generally, CTZ derivatives with multiple hydroxyl groups has less membrane permeability than ones with none or few of a hydroxyl group.

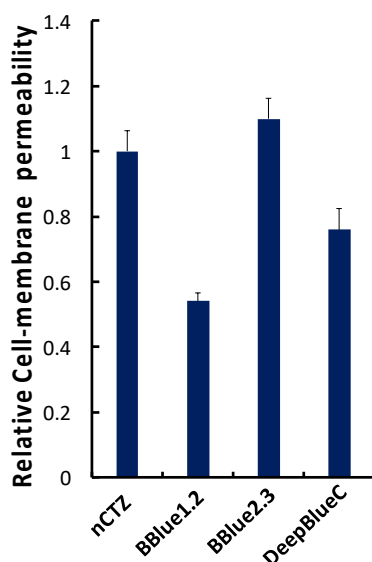


Suppl Figure 5. The relative BLI of live cells transiently expressing RLuc8.6-535SG when combined with CTZ derivatives. **(A)** The BLI in live COS-7 cells expressing RLuc8.6-535SG.

(B) The BLI in live HeLa cells expressing RLuc8.6-535SG.

4.5. Cell membrane permeability assay of CTZ derivatives

BLI from intact COS-7 cells expressing RLuc8.6-535SG or the lysates (lysed using Promega lysis buffer for 15 min) was measured in a 96-well black wall optical-bottom microplate (Thermo Scientific) using an image analyzer (Lumazine FA with PIXIS 1024 CCD camera, Nippon Roper) equipped with an EM-CCD camera. The BLI measurement was initiated immediately after addition of a CTZ derivative (final concentration: 10 μ M) and determined throughout 30 min.



Suppl Figure 6. The cell membrane permeability test of CTZ derivatives. The relative cell membrane permeability was calculated through dividing the BLI of from live COS-7 cells by the BLI obtained from the cell lysate. The cell membrane permeability values are normalized to that of nCTZ/RLuc8.6-535SG pair.

Suppl Table 5. The BL properties of selected CTZ derivatives in living COS-7 cells expressing

RLuc8.6-535SG.

	Total BLI [p/s]	BL-half life time (10 μ M) [min]
BBlue1.2	2.5×10^5	11
BBlue2.3	5.2×10^5	18.5
DeepBlueC	9.7×10^3	7

4.6. Bioluminescence assay in living cells

It is well known that nCTZ penetrates the mammalian cell membrane and quickly diffuse throughout the cytosol [10].

In order to design CTZ derivatives having excellent BL properties in living cells, we need to consider several biophysical factors such as lipid–water partition coefficient (P), subcellular localization of luciferins and efflux from cells. For example, the cLogP values of nCTZ (4.42) and BBlue1.2 (4.29) are very similar to each other, indicating that these two substrates have similar hydrophobic character. However, contrary to our expectation, the cell membrane permeability of nCTZ is much higher than BBlue1.2 (Figure 5B). This discordance can be explained as follow: mammalian cells have a chemical efflux machinery and the CTZ derivatives can be transported out of the cells under this mechanism. Previously, the two membrane transport proteins, ABCB1 and P-glycoprotein (Pgp), have been reported as mediating the efflux of CTZs [11]. Interestingly, Pgp has substrate specificity for nCTZ, CTZ-*f*, CTZ-*h* and CTZ-*hcp*, but not for CTZ-*n* and CTZ-*cp*. Thus, the effects of membrane transport proteins on CTZ efflux may be a reason for the BLI discrepancy between nCTZ and BBlue1.2.

4.7. Optical properties of living mammalian cells stably expressing RLuc8.6-535SG or iRFP-RLuc8.6-535SG with respect to variance in the optical filters, biliverdin (BV) supplementation, BL half decay rates, and luciferin concentration dependency

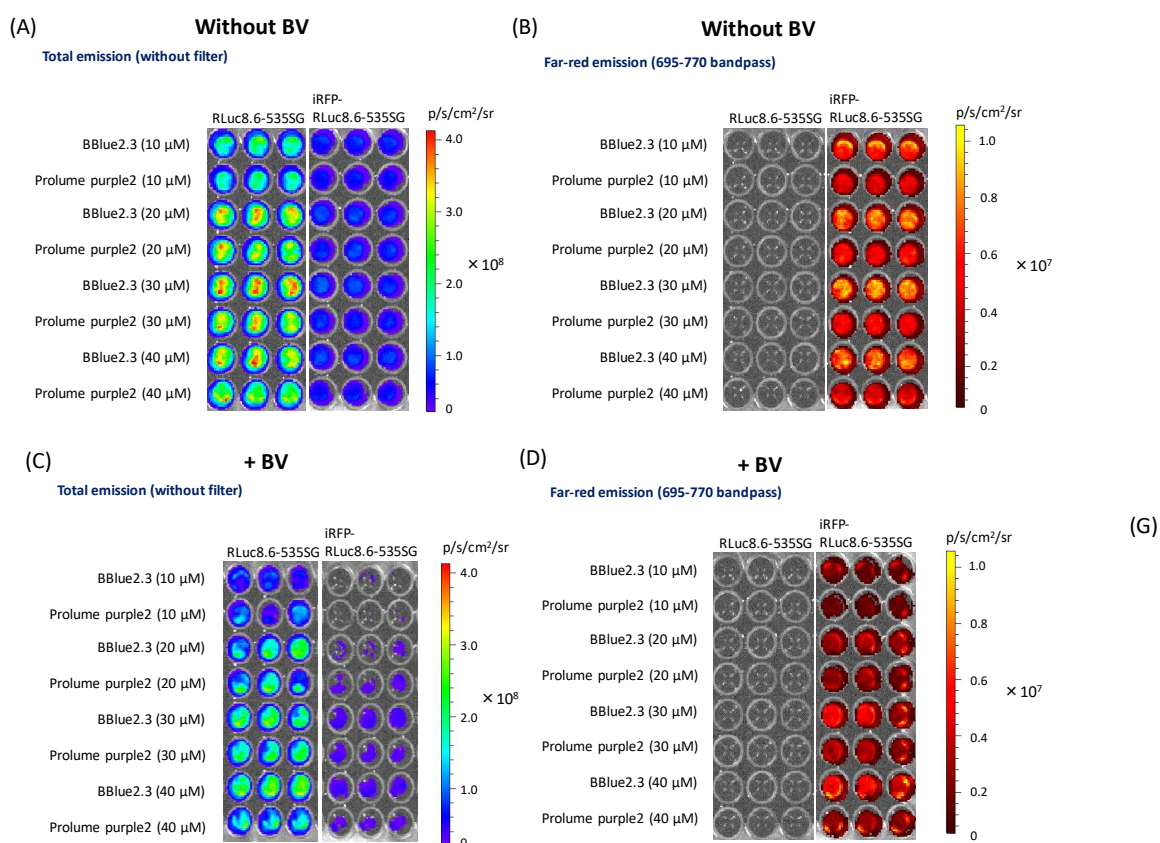
The optical properties of the BL of living mammalian cells stably expressing RLuc8.6-535SG or iRFP-RLuc8.6-535SG were investigated with respect to variance in the optical filters, biliverdin (BV) supplementation, BL half decay rates, and luciferin concentration dependency (Figures 2E -2F; Suppl. Figures 7 -8). The stable cells were plated on 96-well black frame optical-bottom microplates and incubated up to 80% confluency. The cell media were changed with a DMEM medium supplemented with 5% FBS and 1% penicillin/ streptomycin (P/S) mixture, or with a DMEM medium supplemented with 5% FBS, 1% P/S, and 10 μ M BV (final concentration). The microplates were incubated for 5 hours before BL measurements. The BL intensities were determined every 125 seconds with an IVIS optical imaging system with an open filter window or a Cy5.5 band-pass (BP) filter (695-770 nm) immediately after addition of varying concentrations of BBlue2.3 or Prolume Purple 2, which range from 10 – 40 μ M.

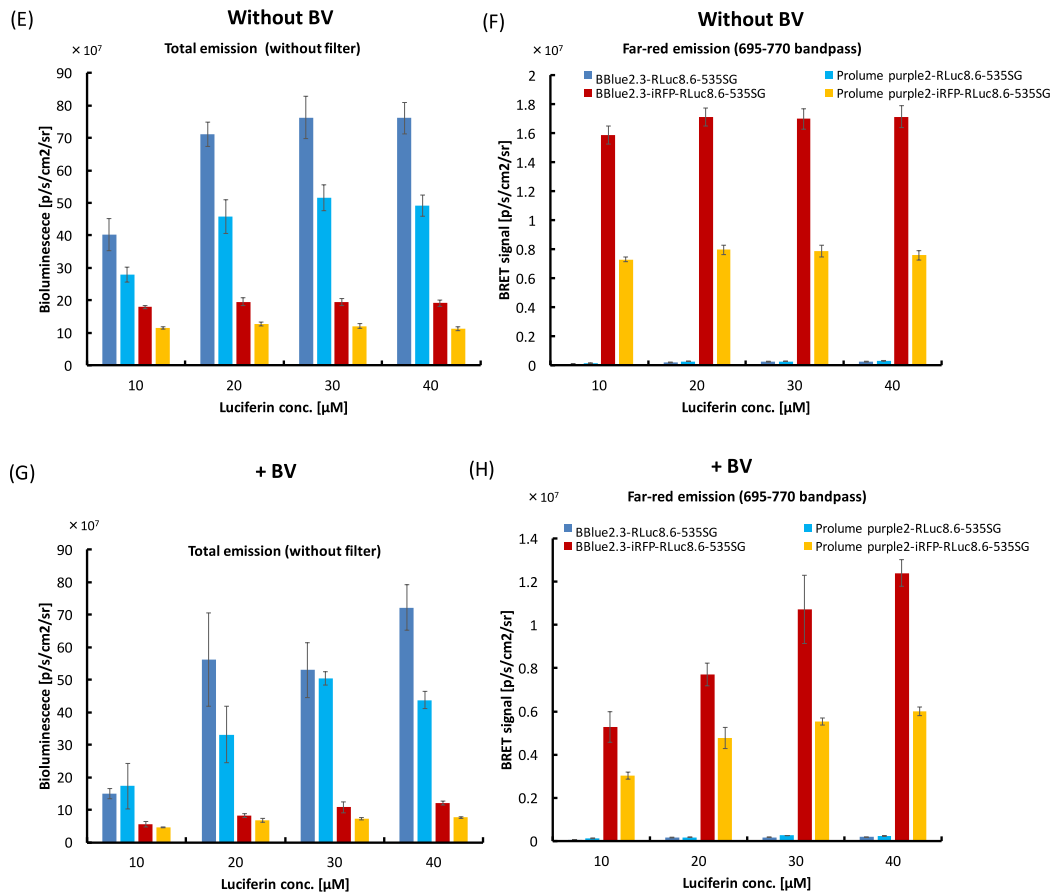
The results show that BV at the applied concentration do not significantly elevate the BLI, which is also observed with similar *in vivo* studies. It is considered that endogenous BV in the serum contributed to form the fluorophore of iRFP. Based on the results, we did not supplement further BV in the culture medium hereafter.

The BLI comparison with open and Cy5.5 BP filter indicates that RLuc8.6-535SG mostly emits BL in a visible region, and thus the BL is completely blocked by Cy5.5 BP filter. On the other hand, iRFP-RLuc8.6SG emits a large portion of NIR BL, the BL intensities of which were significant even with Cy5.5 BP filter. The BL intensities passed through the Cy5.5 filter are considered as the BRET signals between iRFP and RLuc8.6-535SG.

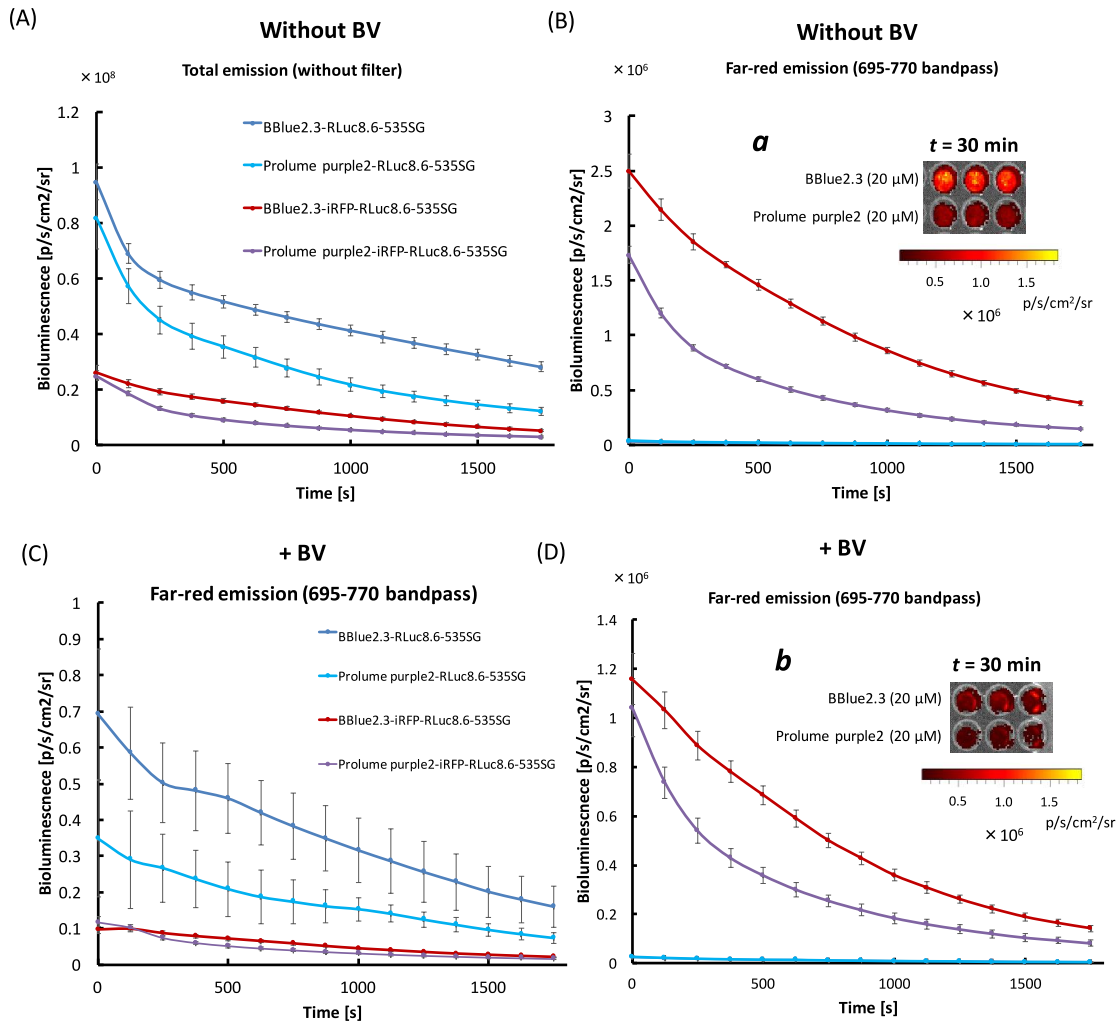
Upon comparison of the substrates, BBlue2.3 emits NIR BL over 2-fold brighter than Prolume Purple 2. The NIR BL intensities of BBlue2.3 did not vary significantly in the range of 10-40 μM . Thus, 10 μM of BBlue2.3 was used for cell-based studies hereafter.

The study on the BL decay rates shows that BBlue2.3 has ca. 30-50 % prolonged BL intensities compared to Prolume Purple 2. This superb optical stability was commonly observed throughout the experimental conditions: i.e., with and without BV; with open or Cy5.5 filters.





Suppl Figure 7. The pseudocolor images showing the substrate dose-dependent BLIs in living cells stably expressing RLuc8.6-535SG or iRFP-RLuc8.6-535SG. The cells were cultured in biliverdin (BV)-supplemented or mock-supplemented medium. **(A)** The optical images without BV and acquired with open window. **(B)** The optical images without BV and with Cy5.5-filter (695-770 nm). **(C)** The optical images with BV and with open window. **(D)** The optical images with BV and with Cy5.5-filter. **(E)** The quantified results of panel (A). **(F)** The quantified results of panel (B). **(G)** The quantified results of panel (C). **(H)** The quantified results of panel (D).



Suppl Figure 8. Time course of the BLIs of MDA-MB231 cells stably expressing RLuc8.6-535SG or iRFP-RLuc8.6-535SG after injection of 20 μM BBlue2.3 or Prolume Purple 2 with open window or Cy5.5 filter. **(A)** Time course without BV and with open window. **(B)** Time course without BV and with Cy5.5 filter. **(C)** Time course with BV and with open window. **(D)** Time course with BV and with Cy5.5 filter. Inset **a** and **b** indicate the pseudocolored images at $t = 30 \text{ min}$, respectively.

5. Docking simulation study

5.1. Molecular dynamic simulations for free energy calculations of ligand binding

The computational docking simulation was performed with AutoDock 4.2.6 [6] using a crystal structure (PDB ID: 2PSJ) of an 8-mutation variant of RLuc (RLuc8) [4], which includes the coelenteramide (CTMD) within the structure (Suppl. Figures 9 and 11). The molecular structures of nCTZ and BBlue1.2 were generated with Avogadro numbers [12]. Each docking simulation was performed 1500 times. Ligand docking poses of CTZ and BBlue1.2 were selected based on the binding energies $\Delta G_{\text{docking}}$ calculated by the AutoDock internal scoring function, their relative orientation and location to the CTMD within the crystal structure.

Absolute binding free energies ΔG_{calc} were calculated using the alchemical thermodynamic cycle [13]. All molecular dynamics simulations were performed using GROMACS 5.1.2 [14]. The RLuc8 with a docked ligand was solvated with the TIP3P water model [15] in a dodecahedral box with minimum distance of 1.2 nm from the protein (number of water molecules were about 13200) and neutralized by adding sodium ions. The missing residues of the RLuc8 structure were modeled using MODELLER [16]. Ligands are parameterized with the general AMBER force field [17] and AM1-BCC point charges [18] using AmberTools14 [19]. The Amber ff99SB-ILDN force field [20] was used for the protein. In the thermodynamic cycle [13], the van der Waals and coulombic interactions of the ligand were turned off using a linear alchemical pathway with $\Delta\lambda = 0.05$ and 0.1, respectively. A softcore potential was employed for the van der Waals interactions transformed [21]. Additionally, 12 non-uniformly distributed λ values (0.0, 0.01, 0.025, 0.05, 0.075, 0.1, 0.15, 0.2, 0.3, 0.5, 0.75, 1.0) were used for the ligand restraints to prevent the ligand leaving the binding site when the ligand–protein interactions are turned off. The relative position and orientation of the bound ligand with respect to the protein was restrained by means of one distance with force constant of $1,000 \text{ kcal mol}^{-1} \text{ nm}^{-2}$, two angles and three dihedral harmonic potentials with force constant of $10 \text{ kcal mol}^{-1} \text{ rad}^{-2}$. The contribution of the restraints to the free energy was calculated analytically [22].

Therefore, the complex simulations (ligand and protein in solution) with 41 windows and the ligand simulations (ligand in solution) with 31 windows were performed. Each window was first energy minimized for 5000 steps followed by 0.5 ns NVT constant and 1.0 ns NPT constant simulations for equilibration with the protein backbone particle restrained (force constant of $1000 \text{ kJ mol}^{-1} \text{ nm}^{-2}$). The time step was set at 2 fs. The temperature of 298.15 K was controlled with Langevin dynamics [23, 24]. The pressure of 1 bar was controlled with Berendsen barostat [25] in the equilibrium simulations. Thereafter, 10 ns unrestrained production runs were performed using Hamiltonian exchange Langevin dynamics at NPT constant, where the pressure of 1 bar was controlled with the Parrinello-Rahman barostat [26]. In order to enhance sampling of uncorrelated configurations, we used the Gibbs sampling scheme [27], where 3 million swaps between replica pairs were attempted every 1,000 time steps. Electrostatic interactions were calculated using the particle mesh Ewald (PME) algorithm [28] with a real space cut-off of 1.2 nm, a spline order of 6, a relative tolerance of 10^{-6} , and a Fourier spacing of 0.1 nm. The switching function was applied for the van der Waals interactions between 1.0 nm and 1.2 nm. All the H-bonds were constrained using the P-LINCS method [29, 30]. The long-range dispersion correction was applied [31]. For the free energy estimation, the results were analyzed using the multiple Bennet acceptance ratio (MBAR) [32]. The first 1 ns of each window was discarded as a non-equilibrium period. Figures were prepared with CueMol (<http://www.cuemol.org>).

5.2. Study results of docking simulation study

A previous docking simulation of nCTZ to the lower portion of the RLuc8 active site including the putative catalytic amino residue, indicated that the hydroxyl group at the C-6 position binds to these residues (H285, E144 and D120) via hydrogen bonding and it might strongly affect the enzyme

activity[3, 4]. In order to elucidate the enzymatic recognition mechanism of nCTZ and BBlue1.2 by RLuc derivatives, a computational docking simulation of the CTZ with RLuc8 was conducted using Autodock4.2.6.

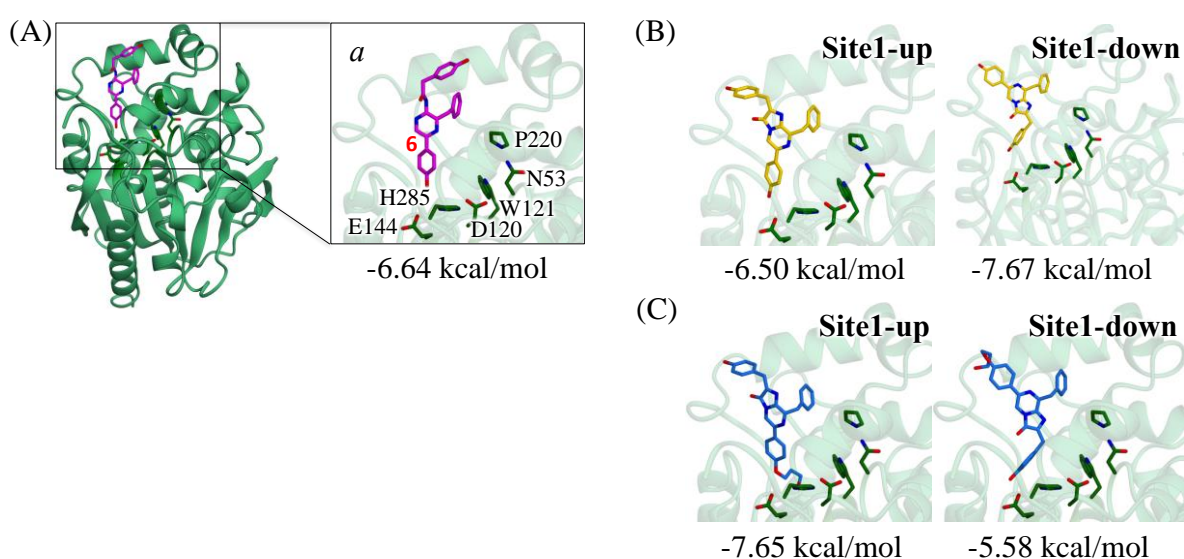
As mentioned before, the position of CTMD in the RLuc8 crystal structure presented a “secondary binding” position and not the position of the CTMD/CTZ during the enzymatic recognition. Therefore, the current work was also conducted through docking simulation of each CTZ in a “secondary binding” position to investigate the most stable conformation of BBlue1.2 in the luciferase (Suppl. Figure 10C). First, we estimated the absolute binding free energies of CTMD ($\sim 6.64 \pm 0.12$ kcal/mol) and nCTZ ($\sim 6.50 \pm 0.10$ kcal/mol). The obtained results are very similar, indicating that this docking simulation result of nCTZ/RLuc8 complex is valuable (Suppl. Figures 10AB and Table S2). Then, the relative orientation of the bound nCTZ with respect to RLuc8 was calculated. The most stable conformation regarding the orientation (Suppl. Figure 10B: Site-1-up and Site-1-down) of nCTZ indicates that nCTZ can advantageously insert into the catalytic active site as a binding pose of site-1-down formation ($\sim 7.67 \pm 0.11$ kcal/mol), in other words, the C-6 phenyl group of nCTZ may protrude from the active site pocket. However, it is also possible that the C-6 phenyl group of nCTZ can insert into the active site pocket as a binding pose of site-1-up ($\sim 6.50 \pm 0.10$ kcal/mol), because the accuracy of this ligand-protein complex associated calculation is $1.0 \text{ kcal mol}^{-1}$ [13]. Actually, nCTZ with familiar RLuc derivatives (RLuc8 and RLuc8.6-535) showed two emission peaks (Suppl. Figure 2), a red-shifted major shoulder around 500-550 nm and a blue-shifted shoulder at 390 nm, which indicates that the CTMD in the excited state can form at least three light-emitting intermediates during the enzymatic reaction. The formation of the phenolate anion and the pyrazine anion CTMD gives rise to the red-shifted emission around 480 nm and 530 nm, respectively. On the other hand, the blue-shifted emission originates from the neutral CTMD

form, due to the incomplete deprotonation of the *p*-hydroxyl group at the C-6 phenyl group of nCTZ. Because the emission colors greatly depend on its interaction with amino acid residues in the catalytic active site of the luciferase, nCTZ is perhaps captured by RLuc derivatives in both orientations of the binding poses (the configuration of site1-up and site-1-down) inside the enzyme pocket illustrated in Suppl. Figure 10B, resulting in two emission peaks. Interestingly, nCTZ shows differences in the BL emission wavelength with RLuc8, RLuc8SG, RLuc8.6-535 and RLuc8.6SG (Suppl. Figures 10 and 11). Therefore, it can be assumed that the C-6 hydroxyl group interacts with different amino acid residues inside the active site of the RLucs.

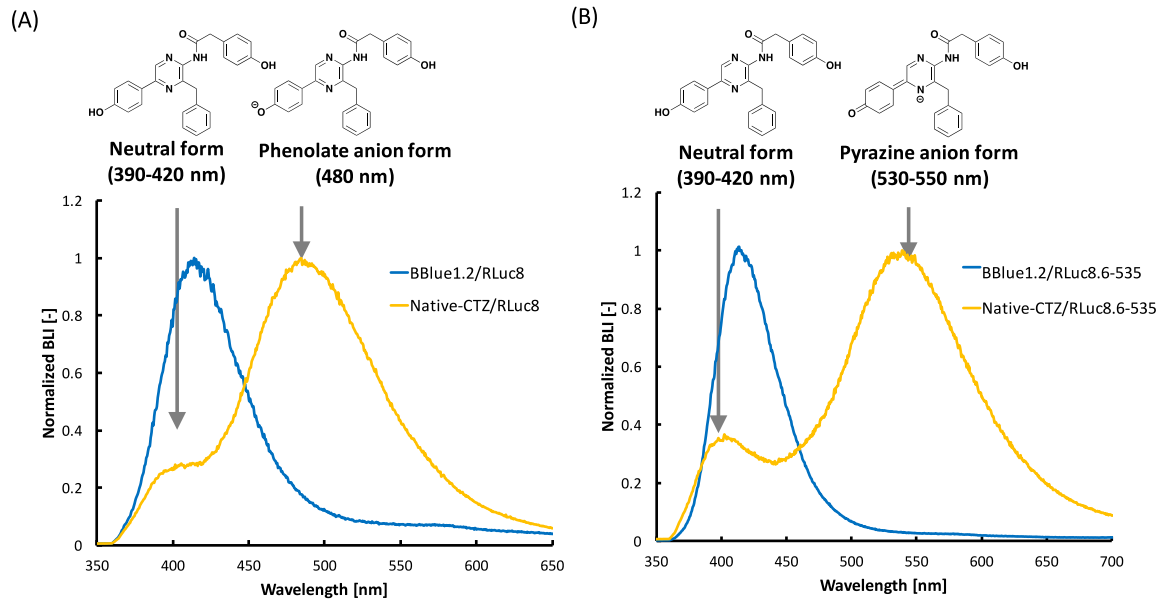
Next, we calculated the relative orientation of the bound BBlue1.2 with respect to RLuc8 and the results are shown in Suppl. Figure 10C. As a result, the configuration of site-1-up ($\sim 7.65 \pm 0.14$ kcal/mol) is preferred for BBlue1.2 inside the active site, which implies that in the most stable conformation, the alkyl linker moiety at the C-6 position of BBlue1.2 may insert into the catalytically active site of RLuc8 and has a hydrophobic and/or hydrogen bond interaction with the amino acid residues. Therefore, the docking simulation results suggest that the size and shape of the C-6 substituent of nCTZ strongly affects BLIs.

Suppl Table 6. Summary of the ligand binding energies of selected CTZ derivatives with RLuc8; absolute binding free energies ΔG_{calc} and binding energies with AutoDock internal scoring function $\Delta G_{\text{docking}}$. The unit of all values is kcal/mol. The site1 is near the binding site of coelenteramide (CTMD) within the crystal structure, while site 2 is near the amino acids (N53, D120, W121, E144, P220, and H285) which have mutagenesis affection on the enzymatic activity [33] [34]. In the up pose, the five-membered ring faces the inside of the binding site, whereas in the down pose outward. Snapshots of the binding poses are shown in Suppl. Figure 6.

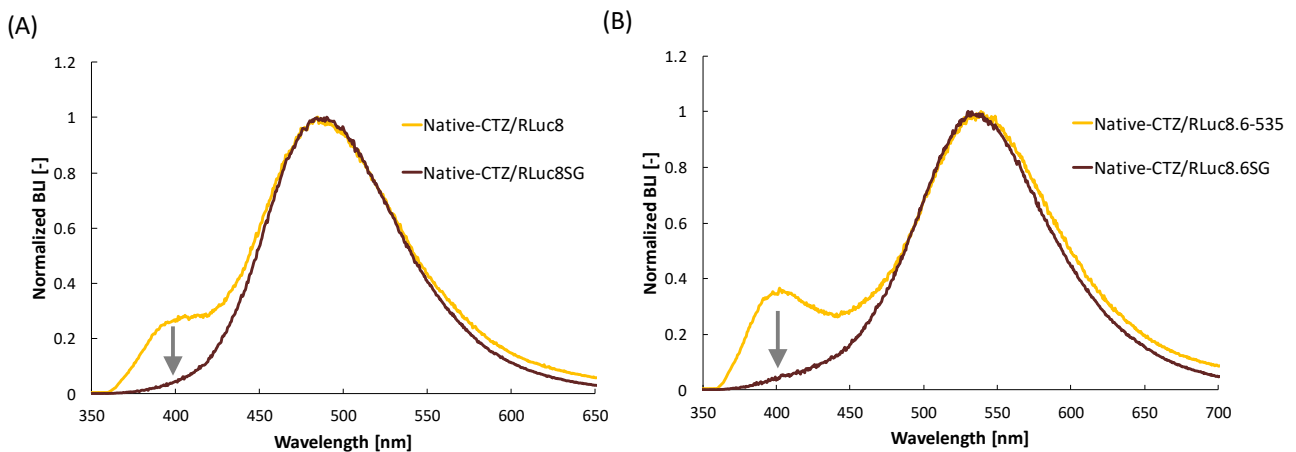
Ligand	Site-1-up	Site-1-down
nCTZ (ΔG_{calc})	$\sim 6.50 \pm 0.10$	$\sim 7.67 \pm 0.11$
BBlue1.2 (ΔG_{calc})	$\sim 7.65 \pm 0.14$	$\sim 5.58 \pm 0.11$
Coelenteramide (ΔG_{calc})	$\sim 6.64 \pm 0.12$	-

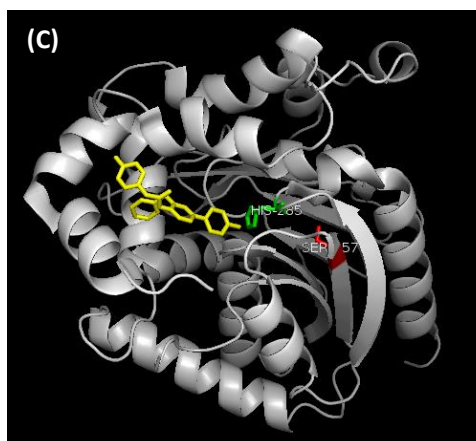


Suppl Figure 9. Binding poses predicted with the docking simulation **(A)** Crystal structure of the RLuc8 with the coelenteramide (CTMD). Inset `a` is a close-up view of the binding site with 6 residues, which have mutagenesis affection on the enzymatic activity. Binding poses of **(B)** the native and **(C)** the BBlue1.2. The absolute binding free energies are specified at the bottom of the close-up views as a reference.



Suppl Figure 10. (A) BL spectra of nCTZ and BBlue1.2 with RLuc8, **(B)** BL spectra of nCTZ and BBlue1.2 with RLuc8.6-535. In contrast to nCTZ, BBlue1.2 causes an incomplete deprotonation of the *p*-hydroxyl group at the C-6 position, resulting in blue-shifted emission.





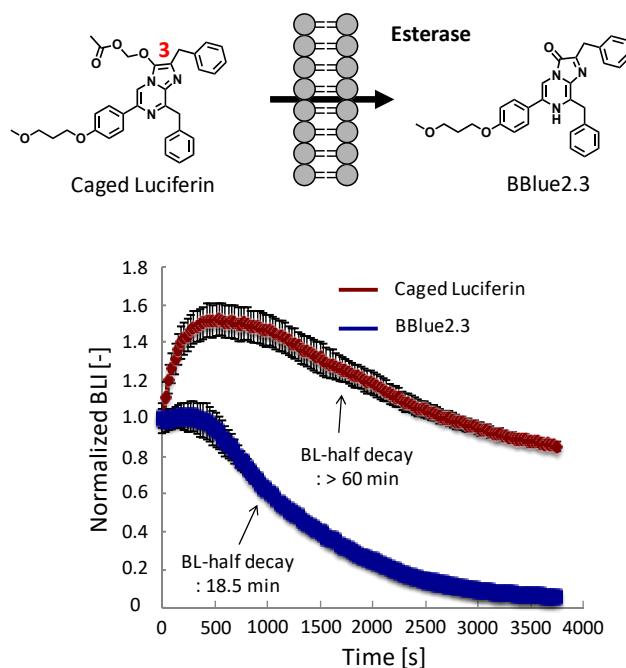
Suppl Figure 11. (A) BL spectra of native CTZ (nCTZ) with RLuc8 and RLuc8SG, **(B)** BL spectra of nCTZ with RLuc8.6-535 and RLuc8.6SG. **(C)** Crystal structure of RLuc8 (PDB 2PSD). The CTMD, His285 and Ser257 (mutation site) are colored yellow, green and red, respectively.

6. Bioluminescence assay with a caged CTZ derivative

Chemical stability of CTZ derivatives is an important factor for BL imaging. An introduction of a protecting group called “cage” to a CTZ derivative can be a solution for prolonged BLI and stability. For this purpose, we speculated that the BL-half decay of BBlue2.3 can be extended by introducing an acetoxymethyl group into the reaction site of the CTZ’s imidazopyrazinone backbone (C-3 carbonyl moiety). The deprotection of the acetoxymethyl group of the caged BBlue2.3 spontaneously occurs by endogenous esterases, which release BBlue2.3 to react with luciferase inside living cells (Suppl. Figure 12). The BL-half life time of CTZ derivatives were characterized as already explained above.

The results show that the greatly prolonged BL decay is observed with acetoxymethyl-BBlue2.3 (Caged Luciferin), compared to that with intact BBlue2.3. The BL half decay times with the Caged

Luciferin and the intact BBlue2.3 was over than 60 minutes and 18.5 minutes, respectively.



Suppl Figure 12. Bioluminescence (BL) emission decay of acetoxymethyl-BBlue2.3 (Caged Luciferin) and intact BBlue2.3 in live COS-7 cells.

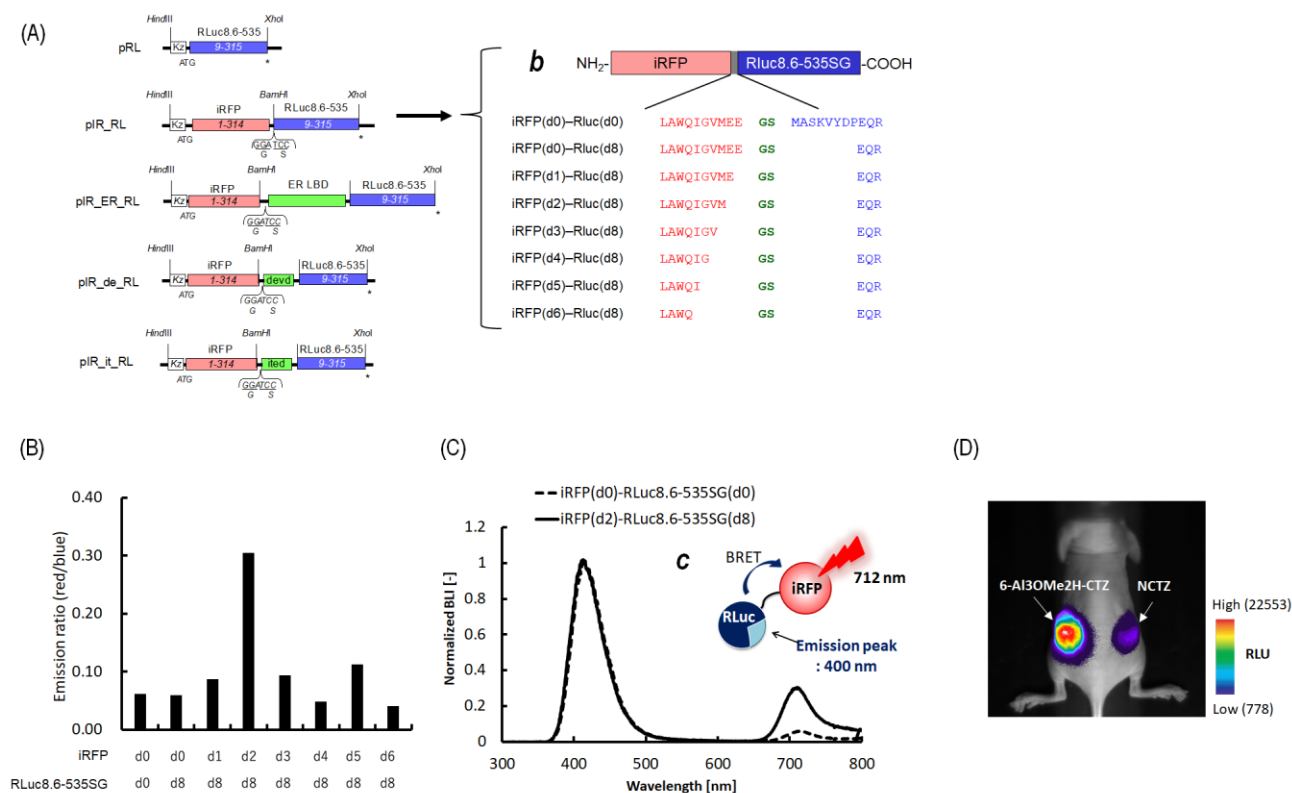
7. Development of optimal BRET imaging probes for NIR bioluminescence imaging

As an initial study for fabricating an optimal BRET imaging system, we examined the optimal linkers between iRFP and RLuc8.6-535SG (Figure 3A; Suppl. Figure 13). The C-terminal end of iRFP and N-terminal end of RLuc8.6-535SG were consecutively eliminated. Every deleted version of iRFP was named d0, d1, d2, d3, d4, d5, and d6, according to the dissected numbers of amino acids. The deleted version of RLuc8.6-535SG was named d8 as shown in Suppl. Figure 13A.

We further examined the spectral match between the deleted versions of iRFP and RLuc8.6-535SG for the efficient BRET. The results show that iRFP(d2)/RLuc8.6-535SG(d8) pair shows the best BRET efficiency (Figure 3B and Suppl. Figure 13B).

The BRET spectra of iRFP(d0)-RLuc8.6-535SG(d0) and iRFP(d2)-RLuc8.6-535SG(d8) were compared for highlighting the improved BRET efficiency (Suppl. Figure 13C). The BRET peak at 717 nm was ca. 4-fold increased by adapting iRFP(d2)-RLuc8.6-535SG(d8), instead of iRFP(d0)-RLuc8.6-535SG(d0).

The BLIs of two CTZ derivatives (nCTZ and BBlue2.3) with iRFP-RLuc8.6-535SG were further compared in a living mouse (Suppl. Figure 13). First, COS-7 cells grown in DMEM supplemented with 10% FBS were transiently transfected with pcDNA3.1(+) plasmids encoding iRFP-RLuc8.6-535SG. After incubation for 48 h, the cells were harvested, washed once, and resuspended in HBSS buffer. The cells were counted before experiments using a cell counting chamber (Burker-Turk Deep, Erma Tokyo). An equivalent amount (50 μ L) of cells (1.83×10^6 cells/mL) were subcutaneously (*s.c.*) implanted on the back of living mice (BALB/c nude mouse, female, 4-week-old). The BLI was integrated for 1 s immediately after *s.c.* injection of 50 μ L of the CTZ derivatives (20 μ M) into the mice using a Lumazone FA system with an electron multiplying charge-coupled device (EM-CCD) camera (Nippon Roper) (final luciferin concentration, 20 μ M).



Suppl Figure 13. (A) Schematic diagram of cDNA constructs showing detailed domains in coding each fragment. Abbreviations: iRFP, infrared fluorescent protein; Kz, kozak sequence; ER-LBD, the ligand binding domain of human estrogen receptor. Inset **b** shows an iRFP-RLuc8.6-535SG protein with a highlighted junction region between iRFP and RLuc8.6-535SG. The fusion protein consists of iRFP and RLuc8.6-535SG, which were linked with a variable length of linkers G, S for the highest BRET efficiency. **(B)** The effect of the deletion of amino acids in the junction region on BRET efficiency. The bar graph shows the relative optical intensities according to the deletion of amino acids in the junction region. **(C)** The comparison of BRET spectra of two proteins "iRFP(d0)-RLuc8.6-535SG(d0)" and "iRFP(d2)-RLuc8.6-535SG(d8)". Inset **c** illustrates that schematic diagram of BRET proteins consisting of iRFP and RLuc8.6-535SG. **(D)** The BRET-based image obtained using nude mice subcutaneously (s.c.) implanted with the same amounts of COS-7 cells (1.83 ×

10^6 cells) expressing iRFP-RLuc8.6-535SG with BBlue2.3 (left dorsal) and native-CTZ (nCTZ) (right dorsal)}. The luminescence image was taken at 1 s exposure time using Lumazon FA imaging system (Nippon Roper).

8. Discussion on BRET efficiency

It is well known that the BRET efficiency is greatly influenced by energy transfer rate constant ($k_T(r)$), which can be calculated by following equation ^[35].

$$k_T(r) = \frac{q_D \kappa^2 9000(\ln 10)}{\tau_D r^6 128\pi^5 N n^4} J(\lambda)$$

where the q_D value is the luminescence quantum yield (QY) of the BRET donor, n is the refractive index of the medium, N is the Avogadro number, r is the distance between BRET donor and acceptor, τ_D is the life-time of the excited BRET donor, $J(\lambda)$ is the overlap integral representing the degree of overlap of the donor emission spectrum with the acceptor absorption spectrum, and κ^2 is the orientation factor. The authors assume the r in our study is ~ 5 nm for iRFP-RLuc8.6-535SG and is ~ 7.5 nm for iRFP-ER-RLuc8.6-535, considering the reference data on the average distance between FP and RLuc8 [36] [37]. The $J(\lambda)$, q_D and κ^2 values are crucial factors when it comes to select a luminescent protein for BRET. The $J(\lambda)$ value between RLuc8.6-535SG and iRFP was found to be $0.882 \times 10^{15} \text{ nm}^4 \text{ M}^{-1} \text{ cm}^{-1}$ with a specific software, ale version 2.2. According to the relative QY values from Suppl. Table 3, BBlue1.2 displays an approximately 10-fold larger luminescence QY than a representative blue-shifted CTZ derivative, DeepBlueCTM. As for the κ^2 value, we found the appropriate linker (two amino acid residues, G and S) by evaluating the 717 nm/413 nm ratio, which expresses BRET efficiency. Therefore, among all parameters indicated in the above equation,

the optical property of the BRET acceptor most strongly influences the $J(\lambda)$ value.

$$J(\lambda) = \frac{\int_0^{\infty} F_D(\lambda) \varepsilon_A(\lambda) \lambda^4 d\lambda}{\int_0^{\infty} F_D(\lambda) d\lambda}$$

Where $F_D(\lambda)$ is the donor emission at the emission wavelength (λ), and ε_A is the acceptor's molar absorption coefficient expressed in $M^{-1}cm^{-1}$. From these equations, the relatively low BRET efficiency compared to existing BRET proteins is explained by the relatively low molar absorption coefficient of the acceptor (the molar absorption coefficient of solet band of iRFP: $39,900 M^{-1}cm^{-1}$)

[38]

References

1. Nishihara R, Suzuki H, Hoshino E, Suganuma S, Sato M, Saitoh T, et al. Bioluminescent coelenterazine derivatives with imidazopyrazinone C-6 extended substitution. *Chem Commun.* 2014; 51: 391-4.
2. Nishihara R, Abe M, Nishiyama S, Citterio D, Suzuki K, Kim SB. Luciferase-Specific Coelenterazine Analogues for Optical Contamination-Free Bioassays. *Sci Rep.* 2017; 7: 908.
3. Loening AM, Fenn TD, Wu AM, Gambhir SS. Consensus guided mutagenesis of Renilla luciferase yields enhanced stability and light output. *Protein Eng Des Sel.* 2006; 19: 391-400.
4. Loening AM, Wu AM, Gambhir SS. Red-shifted Renilla reniformis luciferase variants for imaging in living subjects. *Nat Methods.* 2007; 4: 641-3.
5. Saito R, Hirano T, Maki S, Niwa H, Ohashi M. Influence of Electron-Donating and Electron-Withdrawing Substituents on the Chemiluminescence Behavior of Coelenterazine Analogs. *Bull Chem Soc Japan.* 2011; 84: 90-9.
6. Morris GM, Huey R, Lindstrom W, Sanner MF, Belew RK, Goodsell DS, et al. AutoDock4 and AutoDockTools4: Automated Docking with Selective Receptor Flexibility. *J Comput Chem.* 2009; 30: 2785-91.
7. Woo J, von Arnim AG. Mutational optimization of the coelenterazine-dependent luciferase from Renilla. *Plant Methods.* 2008; 4.
8. Giuliani G, Molinari P, Ferretti G, Cappelli A, Anzini M, Vomero S, et al. New red-shifted coelenterazine analogues with an extended electronic conjugation. *Tetrahedron Lett.* 2012; 53: 5114-8.
9. Shimomura O. Bioluminescence. Singapore: World Scientific Publishing Co. Pte. Ltd; 2006.
10. Zhao H, Doyle TC, Wong RJ, Gao Y, Stevenson DK, Piwnicka-Worms D, et al. Characterization of coelenterazine analogs for measurements of Renilla luciferase activity in live cells and living animals. *Mol Imaging.* 2004; 3: 43-54.

11. Pichler A, Prior JL, Piwnica-Worms D. Imaging reversal of multidrug resistance in living mice with bioluminescence: MDR1 P-glycoprotein transports coelenterazine. *Proc Natl Acad Sci U S A*. 2004; 101: 1702–7.
12. Hanwell MD, Curtis DE, Lonie DC, Vandermeersch T, Zurek E, Hutchison GR. Avogadro: an advanced semantic chemical editor, visualization, and analysis platform. *J Cheminform*. 2012; 4: 17.
13. Aldeghi M, Heifetz A, Bodkin MJ, Knappcd S, Biggin PC. Accurate calculation of the absolute free energy of binding for drug molecules. *Chem Sci*. 2016; 7: 207–18.
14. Abraham MJ, Murtola T, Schulz R, Páll S, Smith JC, Hess B, et al. GROMACS: High performance molecular simulations through multi-level parallelism from laptops to supercomputers. *SoftwareX*. 2015; 1–2: 19–25.
15. Jorgensen WL, Chandrasekhar J, Madura JD. Comparison of simple potential functions for simulating liquid water. *J Chem Phys*. 1983; 79: 926–35.
16. Fiser A, Šali A. Modeller: Generation and Refinement of Homology-Based Protein Structure Models. *Meth Enzymol*. 2003; 374: 461–91.
17. Wang JM, Wolf RM, Caldwell JW, Kollman PA, Case DA. Development and testing of a general amber force field. *J Comput Chem*. 2004; 25: 1157–74.
18. Jakalian A, Jack DB, Bayly CI. Fast, efficient generation of high-quality atomic charges. AM1-BCC model: II. Parameterization and validation. *J Comput Chem*. 2002; 23: 1623–41.
19. Case DA, Darden T, III TEC, Simmerling C, Roitberg A, Wang J, et al. *Amber 14*. San Francisco: University of California; 2014.
20. Lindorff-Larsen K, Piana S, Palmo K, Maragakis P, Klepeis JL, Dror RO, et al. Improved side-chain torsion potentials for the Amber ff99SB protein force field. *Proteins*. 2010; 78: 1950–8.
21. Beutler TC, Mark AE, Schaik RCv, Gerber PR, Gunsteren WFv. Avoiding singularities and numerical instabilities in free energy calculations based on molecular simulations. *Chem Phys Lett*. 1994; 222: 529–39.
22. Boresch S, Tettinger F, Leitgeb M. Absolute Binding Free Energies: A Quantitative Approach for Their Calculation. *J Phys Chem B*. 2003; 107: 9535–51.
23. Gunsteren WFV, Berendsen HJC. A Leap-frog Algorithm for Stochastic Dynamics. *Mol Simul*. 1988; 1: 173–85.
24. Goga N, Rzepiela AJ, Vries AHd, Marrink SJ, Berendsen HJC. Efficient Algorithms for Langevin and DPD Dynamics. *J Chem Theory Comput*. 2012; 8: 3637–49.

25. Berendsen HJC, Postma JPM, Gunsteren WFv, DiNola A, Haak JR. Molecular dynamics with coupling to an external bath. *J Chem Phys.* 1984; 81: 3684–90.
26. Parrinello M, Rahman A. Polymorphic transitions in single crystals: A new molecular dynamics method. *J Appl Phys.* 1981; 52: 7182–90.
27. Chodera JD, Shirts MR. Replica exchange and expanded ensemble simulations as Gibbs sampling: Simple improvements for enhanced mixing. *J Chem Phys.* 2011; 135: 194110.
28. Darden TA, York DM, Pedersen LG. Particle Mesh Ewald: An N·Log(N) Method for Ewald Sums in Large Systems. *J Chem Phys.* 1993; 98: 10089.
29. Hess B, Bekker H, Berendsen HJC, Fraaije JGEM. LINCS: A linear constraint solver for molecular simulations. *J Comput Chem.* 1997; 18: 1463–72.
30. Hess B. P-LINCS: A Parallel Linear Constraint Solver for Molecular Simulation. *J Chem Theory Comput.* 2008; 4: 116–22.
31. Shirts MR, Mobley DL, Chodera JD, Pande VS. Accurate and efficient corrections for missing dispersion interactions in molecular simulations. *J Phys Chem B.* 2007; 111: 13052–63.
32. Shirts MR, Chodera JD. Statistically optimal analysis of samples from multiple equilibrium states. *J Chem Phys.* 2008; 129: 124105.
33. Boresch S, Tettinger F, Leitgeb M, Karplus M. Absolute binding free energies: A quantitative approach for their calculation. *J Phys Chem B.* 2003; 107: 9535–51.
34. Van Gunsteren WF, Berendsen HJC. A Leap-Frog Algorithm for Stochastic Dynamics. *Mol Simulat.* 1988; 1: 173–85.
35. Saito K, Chang YF, Horikawa K, Hatsugai N, Higuchi Y, Hashida M, et al. Luminescent proteins for high-speed single-cell and whole-body imaging. *Nat Commun.* 2012; 3: 1262.
36. Dacres H, Wang J, Dumancic MM, Trowell SC. Experimental Determination of the Forster Distance for Two Commonly Used Bioluminescent Resonance Energy Transfer Pairs. *Analytical Chemistry.* 2010; 82: 432–5.
37. Dacres H, Michie M, Wang J, Pflieger KDG, Trowell SC. Effect of enhanced Renilla luciferase and fluorescent protein variants on the Forster distance of Bioluminescence resonance energy transfer (BRET). *Biochem Biophys Res Comm.* 2012; 425: 625–9.
38. Shcherbakova DM, Baloban M, Emelyanov AV, Brenowitz M, Guo P, Verkhusha VV. Bright monomeric near-infrared fluorescent proteins as tags and biosensors for multiscale imaging. *Nat Commun.* 2016; 7: 12405.

